Model Development and Validation of an Industrial UOP Fluid Catalytic Cracking Unit with a High−Efficiency Regenerator

ARTICLE *in* INDUSTRIAL & ENGINEERING CHEMISTRY RESEARCH · JANUARY 2008

Impact Factor: 2.59 · DOI: 10.1021/ie071035b

5 AUTHORS, INCLUDING:

Carla Pinheiro
Technical University of Lisbon
31 PUBLICATIONS **160** CITATIONS

SEE PROFILE

Model Development and Validation of an Industrial UOP Fluid Catalytic Cracking Unit with a High-Efficiency Regenerator

Joana L. Fernandes,[†] Carla I. C. Pinheiro,*[,†] Nuno M. C. Oliveira,[‡] José Inverno,[§] and Fernando Ramôa Ribeiro[†]

IBB—Institute for Biotechnology and Bioengineering, Centre for Biological and Chemical Engineering, Instituto Superior Técnico, Av. Rovisco Pais, 1049-001 Lisboa, Portugal

This work presents an enhanced model for the reactor−regenerator system of a UOP fluid catalytic cracking (FCC) unit with a high-efficiency regenerator. The model is derived from fundamental principles; relative to earlier versions, a different cracking deactivation model is considered, and the freeboard region in the regenerator vessel is also explicitly addressed. The resulting model is fitted to industrial data, using new correlations to estimate the cracking kinetic constants and other important parameters in the FCC heat balance. In the development of these correlations, only routinely available data and operating variables were considered. As demonstrated, parameter estimation allows a good agreement between the simulated results and the available industrial data. The procedure followed can, therefore, be used to adapt this model to different units of the same class. A comparison of the main features of the steady-state and the dynamic behavior of the validated model with previous results is also considered in this paper.

1. Introduction

Over the past 70 years, considerable attention has been dedicated to catalytic cracking, one of the most important processes in a refinery. In fact, it also corresponds to one of the most profitable steps, since it converts low-value, high-boiling feedstocks into valuable products such as gasoline and diesel fuel; in this case, even small improvements can lead to significant economic gains. Extensive research is still being done concerning detailed modeling of specific parts of a fluid catalytic cracking (FCC) unit. However, when the entire unit is considered, often it becomes difficult to retain all of the details of the FCC process and many simplifying assumptions are usually made. These assumptions frequently depend on the type of application for which the model is intended. Here, we are mostly interested in the development of models capable of supporting the real-time supervision of these units. For this purpose, the accurate predictions of both the major steady-state and dynamics characteristics are especially important, especially the ones that are more relevant at the economical level. In addition, these models should have a computational complexity appropriate for real-time applications and preferably should use information that can be considered to be routinely available in a typical refinery.

Several authors[1−12] have previously developed models of FCC reactor−regeneration systems. A brief review of these models can be found by Fernandes et al.,[1] where a model for the R2R FCC unit from Axens/IFP and Stone & Webster is also presented. Although many FCC models can be found in the open literature, comparisons of the results produced with industrial plant data are much scarcer and sometimes reported unclearly. Some authors[2−6] have compared their model predictions with industrial data. However, in all those works, only predictions of regenerator temperature, riser reactor temperature, and gasoline and coke yields are compared to industrial data, and the number of cases used in model validation is very small or is not referred.

It thus becomes readily clear that, while some comparisons of simulated results of FCC models with industrial data are available, in general they do not allow a thorough assessment of the quality of the predictions over a representative set of process variables, for this process. Moreover, considering the previously stated objective of the present work, it is fair to say that these studies are also insufficient to determine the feasibility of using detailed mechanistic models as a supporting tool for real-time supervision of these units. This conclusion can be attributed to several difficulties present in the study of these systems:

- First, and as previously mentioned, it is difficult to find a set of simplifying assumptions to generate a complete model for a FCC unit, with complexity adequate to real-time solution, without introducing significant simplifications that limit the fidelity of the description of the dynamic and static behavior of the individual parts involved.
- Also, the availability of good industrial data, for representative periods of time, can be a limiting factor. Often the variability of the data is due to many unmeasured disturbances (such as the origin and quality of the loads, variations in the catalyst activity, etc.), which are difficult to correlate in mechanistic models, without a posteriori data regression.

This work, therefore, proposes a pragmatic approach to overcome some of the previously pointed difficulties in the construction of fundamental based dynamic models of FCC units with high-efficiency regenerators. In the following part, a modification of the model presented by Fernandes et al.[12] is successfully validated with industrial data from the steady-state balances of a FCC unit equipped with a high-efficiency regenerator. This unit is located in Sines (Portugal) and is operated by Galpenergia. Since only routinely available data and operating variables were considered, this procedure can be used to produce validated models for other FCC units of the

* To whom all correspondence should be addressed. Tel.: (+351) 218417887. Fax: (+351) 218419198. E-mail: carla.pinheiro@ist.utl.pt.

[†] IBB—Institute for Biotechnology and Bioengineering, Centre for Biological and Chemical Engineering, Instituto Superior Técnico, Av. Rovisco Pais, 1049-001 Lisboa, Portugal.

[‡] GEPSI-PSE Group, Department of Chemical Engineering, University of Coimbra, R. Sílvio Lima-Polo II, 3030-790 Coimbra, Portugal.

[§] Galpenergia, Tecnologia e Controlo Processual, Refinaria de Sines, 7520-952 Sines, Portugal.

10.1021/ie071035b CCC: $40.75
Published on Web 01/15/2008

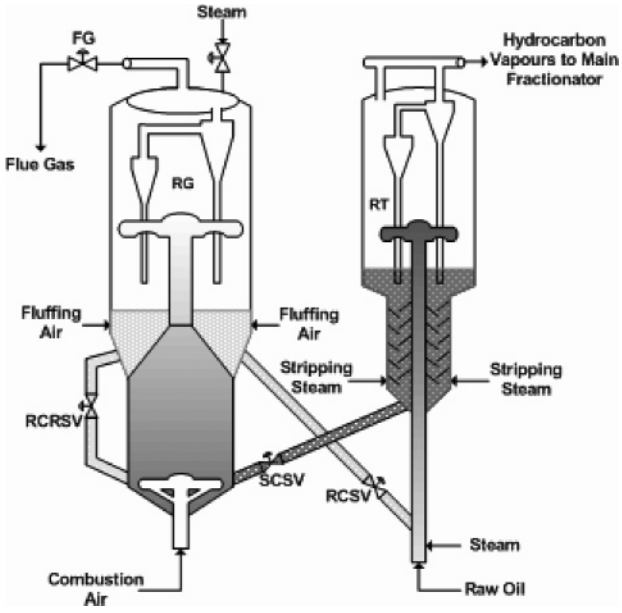

Figure 1. UOP fluid catalytic cracking unit with a high-efficiency regenerator.

same class. The structure of the remaining part of the paper is the following: in Section 2, a brief description of the structure of the model used is given. Details relative to the computer implementation are considered in Section 3. The aspects relative to the determination of the parameters and model validation are considered in Section 4. Finally, in Section 5, a comparison of the main features of the steady-state and dynamic-state behaviors predicted by the validated model are presented and compared with available results.

2. Process Model

A schematic overview of an FCC unit with a high-efficiency regenerator is presented in Figure 1. The FCC unit is composed by the reactor section, which includes a riser, a disengagement vessel, and a stripper, and the high-efficiency regenerator, which is composed by a combustor, a lift, and a regenerator vessel. Two standpipes link the reactor section to the regenerator section.

For better comprehension, the FCC model is divided into parts that correspond to the different components/regions of the FCC unit. The main assumptions made for modeling the reactor section that includes the feed vaporization, the riser, and the disengager/stripper vessel are as follows: instantaneous and complete feed vaporization; pseudo-steady state for the riser, which was modeled as an adiabatic plug-flow reactor with a 6-lump kinetic model; and a CSTR dynamic model for the disengager/stripper vessel. A detailed presentation of these parts of the model can be found in the paper by Fernandes et al.[1]

A previous model for the high-efficiency regenerator was presented by Fernandes et al.[12] In the present work, this model will be used for the section that comprises the combustor and lift, as well as in what refers to the combustion kinetic model. In the lower part of the combustor, mass and energy equilibria are considered to be reached instantaneously, when the two catalyst flows join the air entering the combustor. Here, it is also considered that only mixing of the catalyst and gas streams occurs, without combustion reactions. The upper part of the combustor and the lift were modeled as a plug-flow reactor where most of the combustion reactions take place. Although the catalyst residence time in the combustor and lift is usually about $^1/_4$ of the residence time in the regenerator vessel, it is also about $^1/_{15}$ of the residence time in the disengager/stripper vessel. Therefore, it has been verified by simulation that assuming a pseudo-steady state for the lift and combustor does not significantly affect the global dynamic response of the system, while allowing a faster overall model solution.

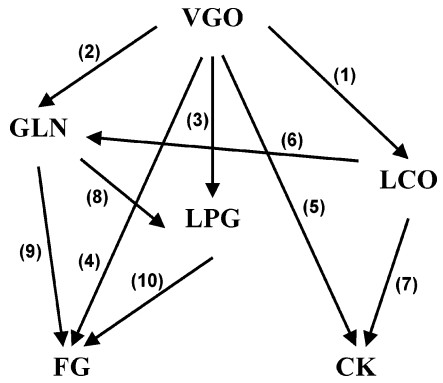

Figure 2. Reaction network with 6-lumps for gas oil catalytic cracking.

The catalyst standpipes link the riser reactor to the regenerator (Figure 1). The catalyst flow rates that go across the standpipes are controlled by the opening of slide valves and the pressure drop across them. For modeling purposes, it was considered that the catalyst flow varies linearly with the valve opening and the pressure differential across the valve, and that there are no reactions inside the standpipes and no mass or heat losses to the surroundings. Since the residence time of the catalyst in the standpipes is of the order of a few seconds, steady state was also considered in this zone.

The next sections address the modifications introduced in the cracking deactivation function of the kinetic model and in the regenerator vessel of the high-efficiency regenerator model.

2.1. Cracking Kinetic and Deactivation Model. The incorporation of appropriate kinetic descriptions of catalytic cracking reactions has probably been one of the major limiting factors in the development of FCC commercial simulators in the last 30 years. The presence of thousands of species, both in the feed and the products, the lack of analytical resources in industry, and the computational effort required make the description of commercial FCC reactions using exact kinetic expressions extremely hard. Therefore, instead of exact kinetics, a number of lumped kinetic schemes have been proposed for FCC modeling.[13−23] In addition, another important fact is the very fast deactivation of the catalyst that does not allow the kinetic reaction rates and the catalyst deactivation to be studied and determined independently from each other.[22−24]

The choice of the kinetic and deactivation models should, therefore, be adequate to the type of usage that the FCC simulator will have. It is also important to keep in mind that it is not realistic to attempt to define a detailed microkinetic model for gas oil industrial cracking, since it would involve hundreds of elementary steps, for which kinetic parameters would need to be determined.[25] Nevertheless, to globally predict the behavior of FCC industrial units, a kinetic model with a detailed product distribution is required.[26] In the paper by Fernandes et al.,[1] a 6-lump model for gas oil cracking adapted from the model for residue cracking first presented by Takatsuka et al.[16] was presented. The lumps considered in this model are as follows: VGO + DO (>360 °C); LCO (220−360 °C); GLN (C_5, 220 °C); LPG (C_3 and C_4); FG (H_2, C_1, C_2, and H_2S); and coke. The reactions between these lumps are presented in Figure 2.

The kinetic rates for reactions 1−10 are given by a typical exponential law, where Φ is the deactivation function:

$$\hat{r}_{ij} = \Phi A_{ij} \exp\left(-\frac{E_{ij}}{RT}\right)\hat{C}_{i,RS}^{n_{ij}} \quad (1)$$

Several equations are available in the literature to model the deactivation in catalytic cracking catalysts, mainly exponential and power laws.[7,20−22,27,28] Although mathematically different, good adjustments against experimental data have been reported, in various cases. Among the equations proposed, two fundamentally different approaches can be found: the *time-on-stream* and the *coke-on-catalyst* functions. Each of these approaches has specific advantages and disadvantages.

Nam and Kittrell[29] addressed this subject and wrote that time-on-stream functions exhibit the advantages of permitting the simultaneous consideration of deactivation mechanisms (e.g., basic nitrogen titration simultaneously with coking) and the formulation of mechanistic coke formation kinetics. Corella and Monzón[30] add that different kinds of coke (whiskerlike, pyrolitic, polymeric, in multilayers, etc.) can be present in the catalyst: although they all contribute to the coke content in the catalyst, they do not contribute equally to deactivation. Therefore, it would be more sensible to use time-dependent relationships (as in the time-on-stream approach), when more than one cause of deactivation is present.

On the other hand, Froment and Bischoff[28] criticize the use of time-on-stream functions and attribute its frequent usage to an easier approach, since a coke content function requires an additional rate equation for the coke formation, in order to be correlated with the process time. From another point of view, Corella and Monzón[30] defend that the results of the coke-on-catalyst approach might depend on what is exactly measured or determined, given the distinct roles that the different types of coke have on deactivation. Nam and Kittrell[29] state, as an advantage, that the use of coke-on-catalyst relationships provides additional insight into the deactivation mechanism, through the inclusion of microbalance data and coke-bed profile data. Furthermore, this type of relationship can be used for catalyst regeneration studies,[29,31] since it accounts for the effect of nonregenerated coke at the riser inlet.

From the perspective of globally simulating the reactor−regenerator system in a FCC, it seems that the advantage of directly accounting for nonregenerated catalyst at the riser inlet, in the deactivation function, is a strong argument relative to the use of a coke-on-catalyst function to describe deactivation. Moreover, as referred by Corella and Frances,[24] another argument that supports this choice is the difficulty in accurately calculating the catalyst time-on-stream, because of the slip between the gas and solid phases in the riser. Therefore, and similarly to other authors,[22,31] we took the general equation proposed by Corella et al.[27] that describes catalyst deactivation. Instead of time-on-stream, we expressed in this case the deactivation against coke-on-catalyst:

$$-\frac{d\Phi}{dY_{ck}} = \alpha\Phi^{d} \quad (2)$$

Here, d is the deactivation order that relates to the number of active sites involved in the global deactivation process.[27] Integrating this equation for $d = 1$, the same deactivation function as used by Fernandes et al.[1] would be obtained. However, Corella et al.[27] have experimentally demonstrated that the deactivation order for industrial feedstocks and commercial catalysts is always superior to 1. Therefore, a different function that describes deactivation is now used, obtained by integration of eq 2 for orders $d > 1$:

$$\Phi = \frac{1}{[1 + (d-1)\alpha Y_{ck}]^{1/(d-1)}}, \quad d \neq 1 \quad (3)$$

Since the deactivation order and constant can change depending on the feedstocks and catalysts, their values will be adjusted to the experimental data considered.

2.2. High-Efficiency Regenerator with Freeboard. In this modified model, the freeboard region in the regenerator vessel will also be included. The importance of modeling the freeboard is mainly related to the rise in temperature of the flue gas due to afterburning reactions and the constraint that it represents in the FCC operation, because of the limited equipment resistance to high temperatures. Hence, the regenerator vessel was modeled as having two distinct regions: the dense bed and the freeboard.

The dense bed is near incipient fluidization conditions and is modeled as a continuous stirred tank reactor (CSTR) in dynamic state. There are still some combustion reactions occurring, however, in a very low extent. Since the concentration of solids is very low in the freeboard and decreases exponentially with height,[32] the presence of catalyst particles was neglected. The freeboard was then modeled as a gaseous homogeneous plug-flow reactor in pseudo-steady state, with the purpose of predicting the temperature in the dilute phase. Gas and catalyst holdups as well as pressure balances were applied to the overall regenerator vessel, by considering it as a CSTR in dynamic state. The pressure in the gas phase was given by the ideal gas law, while the pressure at the bottom of the regenerator vessel was estimated considering the hydrostatic pressure exerted by the catalyst bed. The equations of the mathematical model that describe the regenerator vessel in the high-efficiency regenerator are presented in detail in Section A1 in the Appendix (eqs A1−A27).

3. Model Implementation

The mathematical model of the FCC unit presented in this paper corresponds to a large system of differential and algebraic equations (DAEs) that needs to be solved both in steady-state and transient mode. Table 1 presents the number and type of equations, and variables, for each section of the model. In this count, the variables correspondent to the kinetic parameters, feedstock properties, physical properties, and equipment dimensions were not included. Also, in each zone, the model variables that are relative to other sections, distinct from the one being considered, are described as "known variables", since they might be calculated separately, e.g., sequentially, through iteration of the various model blocks. Table 2 presents a different classification of the model variables, grouped by physical categories. As can be observed, there are 27 degrees of freedom in the model, which can be attributed to operating conditions that must be specified by the user such as inlet stream's flow rates, temperatures, compositions, pressures in adjacent vessels, surrounding conditions, and valve openings that are usually manipulated variables of the FCC regulatory control system. Table 3 presents a typical specification of these operating conditions.

The numerical implementation of the model was done using FORTRAN. Two different strategies were followed, for the steady-state and the dynamic simulations of this unit. In the first case, a sequential modular approach was used for steady-state simulations and data regression, in order to preserve the modular nature of the blocks previously identified and to facilitate the experimentation with different modeling approaches in each block, without incurring the difficulties associated to

Table 1. Numbers of Equations, Variables, and Degrees of Freedom in Each Section of the FCC Mathematical Model

section	known variables, N_{KV}	unknown variables, N_{UV}	algebraic equations, N_{AE}	differential equations, N_{DE}	degrees of freedom, N_{DF}
feed vaporization	7	23	19	0	4
riser	9	65	52	13	0
disengager/stripper	7	33	25	5	3
lower combustor	10	23	16	0	7
upper combustor and lift	10	55	45	10	0
regenerator vessel	10	75	49	16	10
standpipes	4	11	8	0	3
total	57	285	214	44	27

Table 2. Number and Type of Unknown Variables in the FCC Mathematical Model

variable type	symbol	unknown variables N_{UV}
temperature	T	16
heats	H, Q	27
pressure	P, ΔP	25
holdups, levels, & volumes	W, L, V	11
mass & molar flow rates	F, N	80
concentrations	Y, C, $\hat{C}$	27
mass & molar fractions	w, y	40
reaction rate	r, $\hat{r}$	22
volume fraction	ϵ	8
velocity & flux	u, υ, G	11
average properties	ρ, $\bar{M}_w$	9
valve opening	x_v	4
others	Φ, γ, σ, C_D, Re_p	5
total		285

Table 3. Base Case Operating Conditions for the 27 Input Variables Considered

operating conditions	values
fresh feed flow rate, $F_{HC,FF}$ (kg/s)	70.65
fresh feed temperature, $T_{HC,FF}$ (K)	498.15
feed vaporization steam flow rate, $F_{steam,FV}$ (kg/s)	3.16
steam temperature, $T_{steam,FV}$ (K)	653.15
stripping steam flow rate, $F_{steam,ST}$ (kg/s)	1.72
stripping steam temperature, $T_{steam,ST}$ (K)	553.15
combustion air flow rate, $F_{air,CB}$ (kg/s)	56.17
combustion air temperature, $T_{air,CB}$ (K)	458.15
combustion air composition, $y_{i,CB}$ (mol %)	20.7% O_2, 77.7% N_2, 1.6% H_2O, 0% CO, 0% CO_2
regenerator air flow rate, $F_{air,RG}$ (kg/s)	1.16
regenerator air temperature, $T_{air,RG}$ (K)	298.15
regenerator air composition, $y_{i,RG}$ (mol %)	20.7% O_2, 77.7% N_2, 1.6% H_2O, 0% CO, 0% CO_2
pressure in the main fractionator, P_{MF} (kPa)	163.3
pressure in the stack gases, P_{SG} (kPa)	101.3
ambient temperature, T_{surr} (K)	295.15
spent catalyst slide valve opening, $x_{v,SCSV}$ (%)	79.3
regenerated catalyst slide valve opening, $x_{v,RCSV}$ (%)	55.3
recirculated catalyst slide valve opening, $x_{v,RCRSV}$ (%)	99.3
flue gas valve opening, $x_{v,FG}$ (%)	65.1

the global convergence of large sets of differential and algebraic equations (DAEs). The numerical solvers used in this study were as follows:

- ZEROIN: used to find the root of a nonlinear algebraic equation, based on Brent's algorithm.[33]
- DNSQ: used to solve a system of N nonlinear algebraic equations in N variables, by a modification of the Powell hybrid method.[34]
- DASPK: used to solve systems of differential algebraic equations (DAEs) or ordinary differential equations (ODEs) based on Petzold−Gear's Backward Differentiation Formula (BDF) algorithm.[35]

Figure 3 shows the flowchart used in the steady-state solution. After defining the general operating conditions, the model is initiated with approximate conditions of the coke-on-catalyst and the temperature of the regenerated catalyst. Each module is then solved subsequently, using the order presented in this figure, until reaching the regeneration vessel where, new conditions for the regenerated catalyst are computed. These are then compared to the values used in the beginning of the current iteration step; if the difference is higher than the tolerance defined, the solver proceeds to the next iteration step until the tolerances are obeyed and the solver converges to the true steady-state solution. In the range of values considered in this work, convergence was typically observed in <15 iterations of this sequential procedure. Furthermore, the time for solution is always inferior to 1 s (~0.6 s) in a Pentium IV (CPU Intel 3.4 GHz, 1 GB RAM) for a tolerance error less than 10^{-4}. However, while allowing a simple exploratory solution methodology, this procedure should not be inferred as the most efficient strategy that could be devised for the solution of the corresponding system of algebraic equations. For example, a simultaneous solution of the model equations should be considered as a candidate for an efficient implementation in a practical application. However, in this case, the need of using approximate solution methods for model initialization, and the possibility of converging to distinct steady-state values,[12] should be properly considered, in order to avoid significant difficulties both during the solution phase and in the use of the solutions thus produced. The dynamic model simulations were performed using an equation-oriented strategy, usually initiated in steady-state conditions. In this case, the DASPK solver was used.

4. Model Validation

Validation of the previous model was done through parameter estimation using industrial data and subsequent evaluation of the predictive capabilities of the model, with a different data set. To capture the specific properties of the unit and variations in the feedstocks and the catalysts used, new correlations for the cracking kinetic constants are derived. In addition, important feedstock and coke properties for the heat balance such as the cracking enthalpy and the hydrogen-to-carbon molar ratio are also correlated to the set of operating data available.

Other parameters already identified in the model will also be estimated from experimental data. These parameters are the deactivation order, d; the deactivation constant, α; and the fraction of Conradson carbon residue (CCR) that adds to coke, x_{CCR}.

4.1. Model Parameters. It is well-known that feedstock composition as well as the catalyst activity strongly affects the distribution of cracking products. A detailed characterization of a FCC feedstock involves determining both its chemical and physical properties. Because sophisticated analytical techniques,

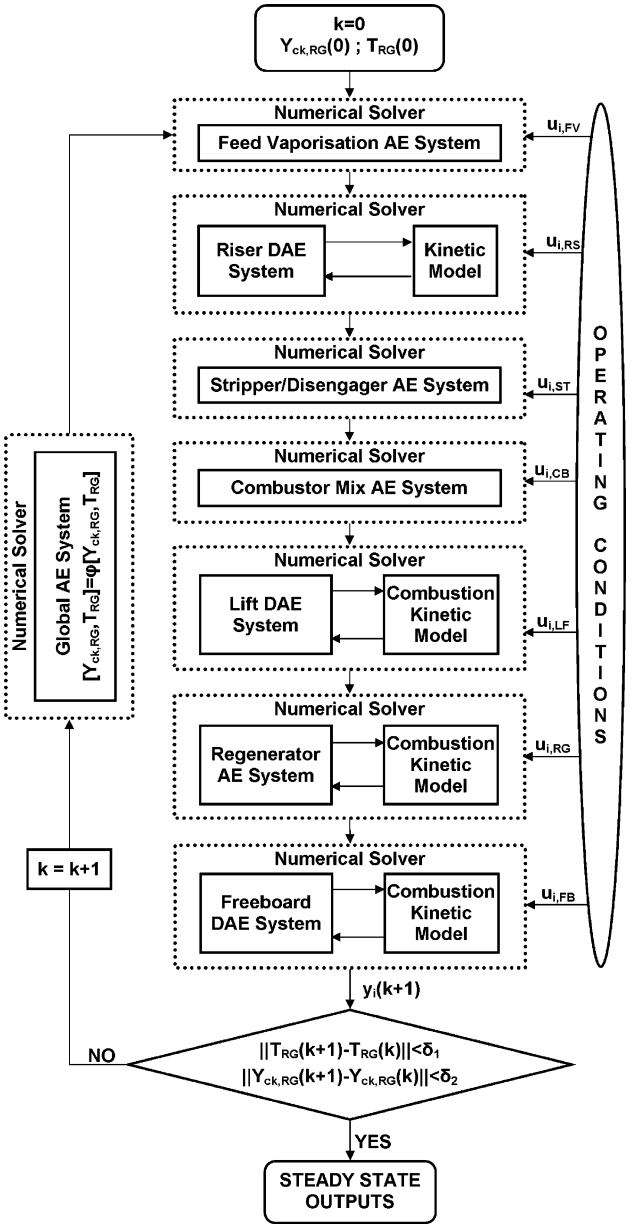

Figure 3. Flowchart for the algorithm solution for the steady-state model.

such as mass spectrometry, are not of practical use on an industrial daily basis, only physical properties are used in this characterization. They provide qualitative measurement of the feed's composition. The properties most widely used by refiners are as follows: °API gravity, distillation data, aniline point, refractive index (RI), bromine number and index, viscosity, and Conradson, Ramsbottom, microcarbon, and heptane insoluble indices.[36] Equilibrium catalyst (E-cat) is also analyzed on a regular basis, since the tests performed on the E-cat can provide valuable information about the physical properties and activity of the catalyst as well as its composition.[36−38]

4.1.1. Cracking Kinetics Parameters. One of the main disadvantages of lumped models is that feedstock composition and catalyst properties are often disregarded. Since the cracking product distribution depends on feedstock and catalyst properties, this means that, every time the feedstock or the catalyst change, a new set of kinetic parameters should be determined.

In order to use the same set of kinetic parameters of a lumped model for a wider range of feedstocks, some authors have proposed correlations for the calculation of the kinetic constants. Voltz et al.[39] presented kinetic constants correlated to the ratio of aromatics to naphtenes. Weekman[14] proposed a three-lump kinetic model, with the rate and catalyst decay constants correlated as a function of the total sulfur and nitrogen contents and carbon distribution evaluated by the n-d-M method, using information reported in the literature about the cracking of 16 different feedstocks. Ancheyta-Juárez et al.[40] proposed correlations for kinetic constants as a function of total sulfur and nitrogen feed contents, aromatics carbons, and paraffinic/naphthenic carbons ratio determined using a method based on refractive index, density, and molecular weight (n-d-m).

In our modified 6-lumps kinetic model, the cracking kinetic constants of vacuum gas oil conversion (VGO) were correlated to feedstock and catalyst properties that are routinely available in the refineries. Since the model is being developed to be used in real-time optimization, all the information required by the kinetic model should preferably be available in each optimizer run. The properties used were then the °API gravity and the sulfur content (*S*) in the feedstock and the vanadium and nickel concentrations in the equilibrium catalyst.

The °API gravity measures the density of a liquid hydrocarbon and is directly related to the specific gravity (SG), which is another common measurement of density at 60 °F (15.5 °C). Compared with specific gravity, °API gravity amplifies small changes in the feed density. The SG relates to °API gravity by the following equation:[36]

$$°\mathrm{API} = \frac{141.5}{\mathrm{SG}(60\ °\mathrm{F})} - 131.5 \tag{4}$$

After studying the variation of industrial product yields with feedstock °API gravity, it was observed that there is a clear effect of the feedstock °API in the yields of light cycle oil (LCO), gasoline (GLN), and liquefied petroleum gases (LPG) (see Figure 4a). A correlation is then proposed for the estimation of the kinetic constants as a function of °API gravity, for the conversion of the feedstock, VGO, into these lumps:

$$A_{ij} = a_{ij} \times °\mathrm{API}^{b_{ij}}, \quad i = \mathrm{VGO\ and}\ j = \mathrm{LCO, GLN, and\ LPG} \tag{5}$$

Although sulfur content in the feedstocks has little effect on the FCC performance, it is an important property, since it appears in the refinery fuel gas (FG) as H_2S (see Figure 4b) and in all catalytically cracked products.[38] FCC feedstocks contain sulfur in the form of organic−sulfur compounds such as mercaptan, sulfide, and thiophenes. However, what is usually determined is the total sulfur expressed as elemental sulfur. This is usually done by the wavelength dispersive X-ray fluorescence spectrometry method (ASTM D-2622).[36] A significant part of sulfur in the feed (∼50%) is converted to H_2S, mainly by the catalytic decomposition of non-thiophenic (non-ring) sulfur compounds.[36]

The estimation of the cracking kinetic constant for the conversion of VGO to FG is then given by a correlation, which is a function of sulfur content in the feedstock:

$$A_{ij} = a_{ij} S^{b_{ij}}, \quad i = \mathrm{VGO\ and}\ j = \mathrm{FG} \tag{6}$$

Crude oil always contains several metals, such as nickel, vanadium, sodium, iron, copper, etc. These metals are concentrated mainly in the heavy boiling range of atmospheric bottoms or vacuum residue and are catalysts themselves, since they promote undesirable reactions, such as dehydrogenation and condensation. Since virtually all of the metals in the FCC

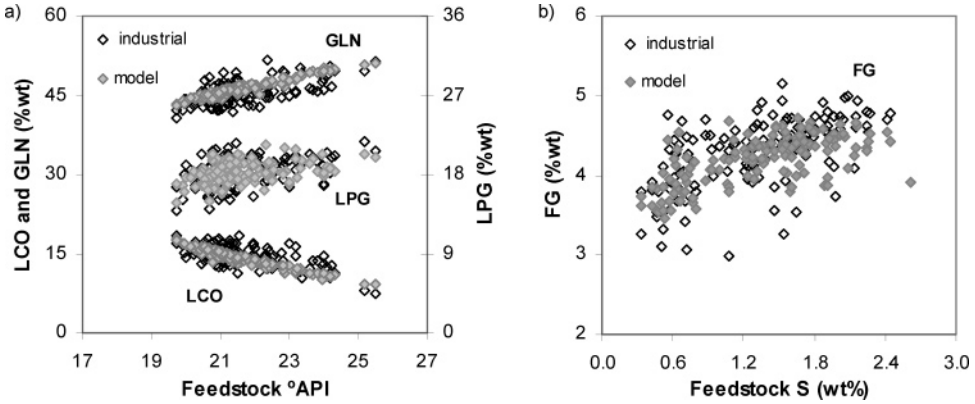

Figure 4. Influence of feedstock properties in the product yields for the data of 136 days: (a) feedstock °API vs LCO, GLN, and LPG yields and (b) feedstock sulfur content vs FG yield.

feedstocks become deposited on the cracking catalyst,[38] the activity and selectivity of the catalyst is reduced or altered, which affects the FCC products distribution.[41] Hydrogen and coke yields are thus increased, and gasoline yields are reduced. To avoid loss of activity and selectivity and increasing levels of metals in the FCC catalyst, it is common practice for refineries to routinely add fresh catalyst and withdraw equilibrium catalyst from FCC inventories.[41] In cases of highly contaminated feedstocks, pretreatment of feedstocks such as hydrotreating and/or demetallating is also considered.[38]

Since nickel and vanadium are usually the major contaminants in FCC feedstocks,[41] this study will only consider the concentration of these two metals in the equilibrium catalyst. Nickel has a high dehydrogenation effect. Vanadium has a much lower dehydrogenation effect; however, unlike nickel, vanadium does not stay on the surface of the catalyst. Instead, it migrates to the inner (zeolite) part of the catalyst and destroys the zeolite crystal structure. As a result, catalyst surface area and activity are permanently lost in this case.[38,41] To predict the activity of vanadium contaminated FCC catalysts, Leuenberger[42] proposed an empirical exponential law function of vanadium concentration in the equilibrium catalyst. Moreover, Larocca et al.[43] proposed a deactivation model that includes the effect of metals content given as nickel equivalent (Ni + $^1/_4V$) through the inclusion of exponential correlations, a function of the metal's level, to calculate the pre-exponential factor and the activation energy.

In this work, corrective terms, k_i, for the activity and selectivity of the catalyst toward each lump, will be multiplied by the rate equations. These terms will account mainly for metals dehydrogenation effects, and they will be expressed by the Mobil metal index, M_{MI},[36] which is a function of vanadium and nickel concentrations in equilibrium catalyst:

$$M_{MI} = \mathrm{Ni} + \frac{\mathrm{V}}{4} \tag{7}$$

$$k_i = M_{MI}^{c_i}, \quad i = \mathrm{LCO, GLN, LPG, FG, and CK} \tag{8}$$

4.1.2. Heat Balance Parameters. In a previous paper, the effects of the uncertainty in the values of the hydrogen-to-carbon molar ratio, H/C, in the coke composition as well as in the cracking enthalpy, ΔH_{crk}, in the riser were addressed.[12] These two properties are fundamental for the heat balance of the FCC unit, and they are both affected by the feed composition, the catalyst properties, and the operating conditions. Therefore, to adjust the model to industrial data, it is essential to estimate these properties. However, since they are not constant and depend on several factors, they were correlated to several operating variables.

The H/C ratio was then correlated to the coke yield at the reactor outlet, since the industrial data showed that this is the variable that mostly influences the values obtained for the coke H/C molar ratio from the heat balances to the unit. Moreover, Wojciechowski and Corma[26] had already observed that H/C decreased with increasing conversion and, consequently, with increasing coke yield. This function is limited both above and below, since it has been observed that the H/C ratio can take values in the range of [0.4, 2.0].[31] An S-shaped function is then proposed, ranging from 0.4 for high coke yields to 2.0 for low coke yields:

$$\mathrm{H/C} = 1.6 \exp(-a_{HC}\mathrm{CK}^{b_{HC}}) + 0.4 \tag{9}$$

The cracking enthalpy was correlated to the riser reactor temperature through a polynomial function:

$$\Delta H_{crk} = a_{\Delta H} T_{RS}^{\ 2} + b_{\Delta H} T_{RS} + c_{\Delta H}, \qquad T_{RS} \geq T_{min} \tag{10}$$

This function is only valid for riser temperatures higher than a certain minimum temperature, T_{min}, since it is expected that the cracking enthalpy increases monotonically with the riser temperature. This minimum temperature is given by the stationary point of eq 10:

$$T_{min} = -\frac{b_{\Delta H}}{2a_{\Delta H}} \tag{11}$$

4.2. Parameter Estimation. Given the previous considerations, 21 parameters for the modified lumped kinetic model need to be estimated from the industrial, where 2 are from the deactivation function, 14 are used to estimate the 10 cracking kinetic constants, and 5 are used to correct the catalyst selectivity/activity for each lump formation. Besides the kinetic parameters, the percentage of Conradson carbon residue, x_{CCR}, also needs to be estimated, since it is not clear what percentage of CCR appears as increased delta coke. These 22 parameters are all related to the products distribution, so they will be estimated by fitting the model to industrial data of the products yields at the riser reactor outlet. The other 5 parameters, which are used to calculate the H/C molar ratio in the coke and the cracking enthalpy, are mostly related to the heat balance and will be estimated from industrial data that concerns the temperatures in the reactor−regenerator system. Therefore, a total of 27 parameters needs to be estimated from the available industrial data (this number is not related to the number of degrees of freedom previously identified, though).

4.2.1. Experimental Data. As previously mentioned, an effort was made to use only routinely available industrial data from an actual operating FCC unit. This can lead to some problems, since the ranges of the operating conditions are quite narrow, making it difficult to obtain parameters with acceptable statistical confidence.

The industrial data used for parameter estimation correspond to a complete group of information on flows, product yields, temperatures, pressures, and feedstock and catalyst characterization for 136 days in a period of 3.5 years of operation of an industrial FCC unit. This unit is installed in Sines (Portugal) and is operated by Galpenergia. From the group of data, 102 days were randomly selected to estimate the model parameters while the remaining 34 days were used for cross-validation. Since there were parameters with very different orders of magnitude, the logarithm of some of the parameters was considered instead.

An alternative source of data that could be proposed for this task is the standard microactivity test (MAT), widely used by researchers to obtain kinetic rate data; this is a standard test, used to compare different catalyst formulations and the effects of potential poisons. However, these MAT tests are not appropriate to obtain kinetic parameters for the models used to simulate commercial FCC units, since MAT conversion does not directly relate to actual FCC conversion.[25]

Besides the MAT system, other laboratory-scale reactors could have been used to provide data for parameter estimation, such as the short contact time reactors.[19] In this case, the intrinsic relations between the process operating variables of an industrial unit are difficult to maintain in a laboratory-scale unit and, as reported for fluid catalytic cracking, the formation of coke is highly dependent on the operating conditions.[36,37] Since the kinetic model presented in this paper is to be used in a FCC unit simulator, a good prediction of coke formation is essential for an accurate overall heat balance of the reactor−regenerator system.

4.2.2. Numerical Method for Data Regression. An adaptive nonlinear least-squares algorithm was used for data regression (DN2FB). This is a modification to the well-known NL2SOL algorithm that allows bounds on the parameters estimated. The algorithm reduces in some cases to a Gauss−Newton or a Levenberg−Marquardt method and is described by Dennis et al.[44] This software is in the public domain and is available from NETLIB.

Parameter estimation was done by minimization of the weighted sum of squares of the residuals between the experimental and model calculated outlet mass fractions and temperatures. A statistical Student's *t*-test was performed on the significance of the individual parameters estimated, with estimation of the confidence intervals. The confidence level chosen was 95%, and the reference value for this probability and distribution is 1.963.

4.2.3. Estimated Parameters. The estimated parameters as well as the corresponding error and the *t*-Student values are given in Table 4. As can be observed, all values show reasonable statistical confidence. The parameters that present lower values for *t*-Student correspond to the secondary reactions 9 and 10 (Figure 2). This is an expected result, since these secondary reactions occur to a much lower extent than the main reactions 1−5. The other parameter with more uncertainty is the percentage of CCR that adds directly to coke. This is not surprising, since, according to the fluid catalytic cracking guide,[38] this percentage is related to the feed nozzle design and operating conditions such as steam injection rates, reactor pressure, and temperature, which means that this percentage is not necessarily a constant, as assumed.

Table 4. Estimated Values of the Model Parameters

parameter	value	*t*-Student
$\log(a_{VGO\rightarrow LCO})$	10.32 ± 0.04	260.3
$\log(a_{VGO\rightarrow GLN})$	6.6 ± 0.1	45.5
$\log(a_{VGO\rightarrow LPG})$	6.2 ± 0.2	26.2
$\log(a_{VGO\rightarrow FG})$	6.9 ± 0.1	48.4
$\log(a_{VGO\rightarrow CK})$	7.6 ± 0.1	51.2
$\log(a_{LCO\rightarrow GLN})$	7.7 ± 0.2	46.2
$\log(a_{LCO\rightarrow CK})$	7.2 ± 0.2	44.6
$\log(a_{GLN\rightarrow LPG})$	12.2 ± 0.2	69.3
$\log(a_{GLN\rightarrow FG})$	10 ± 3	3.5
$\log(a_{LPG\rightarrow FG})$	13 ± 3	4.2
$b_{VGO\rightarrow LCO}$	-1.5 ± 0.1	12.3
$b_{VGO\rightarrow GLN}$	1.62 ± 0.08	20.1
$b_{VGO\rightarrow LPG}$	1.7 ± 0.2	11.6
$b_{VGO\rightarrow FG}$	0.14 ± 0.03	5.2
$c_{i\rightarrow LCO}$	-0.43 ± 0.03	12.9
$c_{i\rightarrow GLN}$	-0.42 ± 0.02	26.3
$c_{i\rightarrow LPG}$	-0.52 ± 0.03	16.5
$c_{i\rightarrow FG}$	-0.22 ± 0.04	4.9
$c_{i\rightarrow CK}$	-0.43 ± 0.03	13.5
d	1.6 ± 0.2	7.8
$\log(\alpha)$	2.9 ± 0.2	19.6
x_{CCR}	0.42 ± 0.09	4.6
$\log(a_{HC})$	-4.84 ± 0.03	177.0
b_{HC}	6.000 ± 0.007	833.5
$\log(a_{\Delta H})$	2.0116 ± 0.0001	1347.0
$\log(b_{\Delta H})$	5.17720 ± 0.00006	9257.0
$\log(c_{\Delta H})$	7.7388 ± 0.0002	3777.0

Table 5. Modified 6-Lumps Kinetic Model for Industrial Catalytic Cracking

$r_{i\rightarrow j}$	$k_j A_{i\rightarrow j}[1 + (d-1)\alpha Y_{ck}^{cat}]^{-1/(d-1)} \exp(-E_i/RT)\hat{C}_i^{n_{ij}}$ [kg/(m^3·s)]
$r_{VGO\rightarrow LCO}$	$2.09 \times 10^{10} M_{MI}^{-0.43}\,^{\circ}\mathrm{API}^{-1.5}[1 + 477 Y_{ck}^{cat}]^{-5/3} \exp(-84.2 \times 10^3/RT)\hat{C}_{VGO}^2$
$r_{VGO\rightarrow GLN}$	$3.98 \times 10^6 M_{MI}^{-0.42}\,^{\circ}\mathrm{API}^{1.62}[1 + 477 Y_{ck}^{cat}]^{-5/3} \exp(-84.2 \times 10^3/RT)\hat{C}_{VGO}^2$
$r_{VGO\rightarrow LPG}$	$1.58 \times 10^6 M_{MI}^{-0.52}\,^{\circ}\mathrm{API}^{1.7}[1 + 477 Y_{ck}^{cat}]^{-5/3} \exp(-84.2 \times 10^3/RT)\hat{C}_{VGO}^2$
$r_{VGO\rightarrow FG}$	$7.94 \times 10^6 M_{MI}^{-0.22} S^{0.14}[1 + 477 Y_{ck}^{cat}]^{-5/3} \exp(-84.2 \times 10^3/RT)\hat{C}_{VGO}^2$
$r_{VGO\rightarrow CK}$	$3.98 \times 10^7 M_{MI}^{-0.43}[1 + 477 Y_{ck}^{cat}]^{-5/3} \exp(-84.2 \times 10^3/RT)\hat{C}_{VGO}^2$
$r_{LCO\rightarrow GLN}$	$5.01 \times 10^7 M_{MI}^{-0.42}[1 + 477 Y_{ck}^{cat}]^{-5/3} \exp(-77.1 \times 10^3/RT)\hat{C}_{LCO}$
$r_{LCO\rightarrow CK}$	$1.58 \times 10^7 M_{MI}^{-0.42}[1 + 477 Y_{ck}^{cat}]^{-5/3} \exp(-77.1 \times 10^3/RT)\hat{C}_{LCO}$
$r_{GLN\rightarrow LPG}$	$1.58 \times 10^{12} M_{MI}^{-0.52}[1 + 477 Y_{ck}^{cat}]^{-5/3} \exp(-146.0 \times 10^3/RT)\hat{C}_{GLN}$
$r_{GLN\rightarrow FG}$	$1.00 \times 10^{10} M_{MI}^{-0.22}[1 + 477 Y_{ck}^{cat}]^{-5/3} \exp(-146.0 \times 10^3/RT)\hat{C}_{GLN}$
$r_{LPG\rightarrow FG}$	$1.00 \times 10^{13} M_{MI}^{-0.22}[1 + 477 Y_{ck}^{cat}]^{-5/3} \exp(-193.0 \times 10^3/RT)\hat{C}_{LPG}$

From Table 4, it is also clear that the °API gravity has, in fact, a strong effect on the GLN and LPG yields, since, in the correlation (eq 5) proposed for the kinetic constants, the exponent coefficients are >1 for GLN and LPG and negative for LCO as expected, since higher °API means that the feedstock is more paraffinic and is expected to produce more GLN and LPG and less LCO. Figure 4a shows that the model predicts well the relation between GLN, LPG, and LCO with feedstock °API. Figure 4b shows that the relation of predicted FG with sulfur content in the feedstock is also in good agreement with industrial data.

A modified lumped kinetic model for industrial catalytic cracking that takes into account feedstock properties as well as metal concentration in the equilibrium catalyst is then proposed

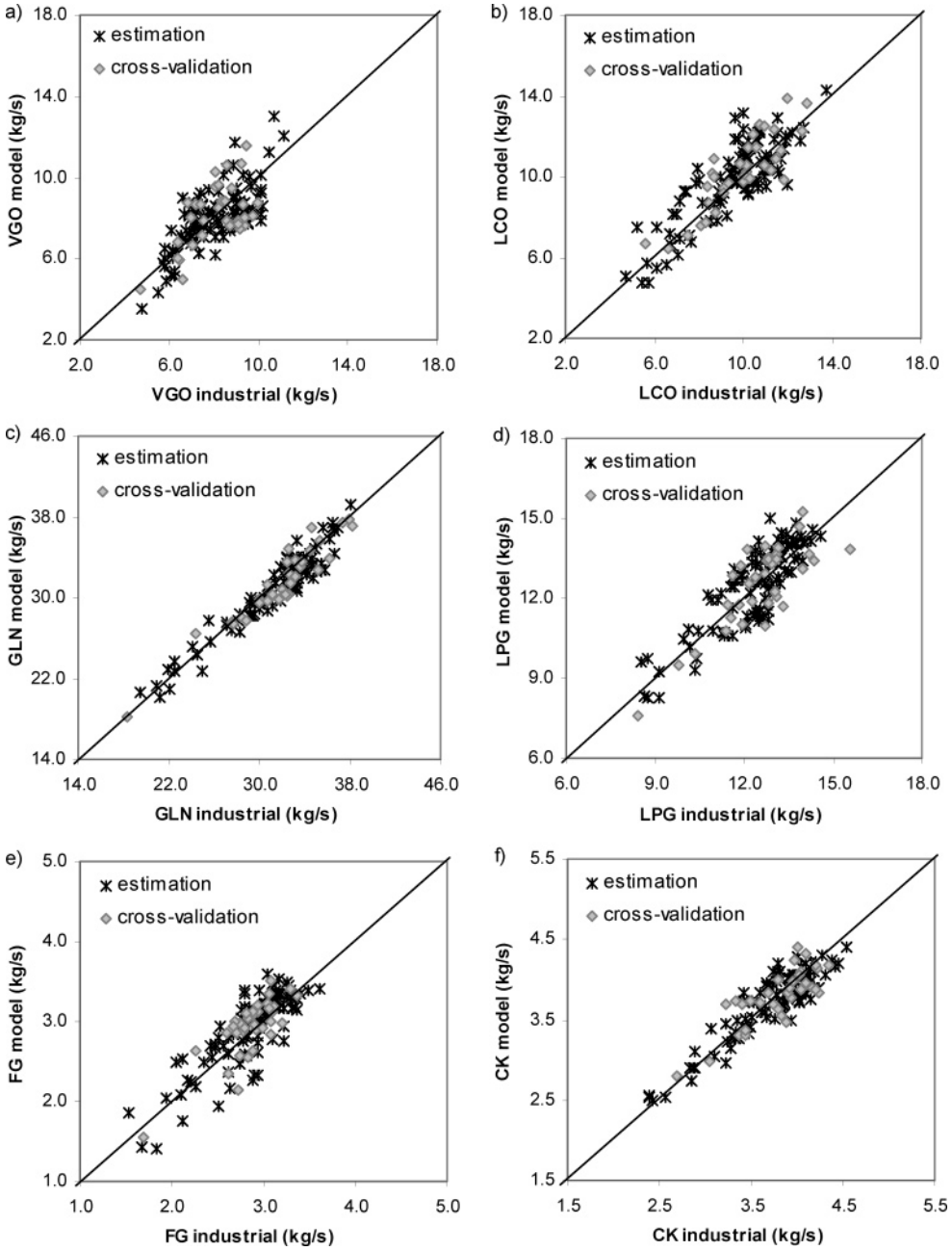

Figure 5. Parity diagrams for the cracking products mass flow rates at the riser reactor outlet, for 102 days of estimation data and 34 days of cross-validation data.

in Table 5. The results obtained for the product distribution at the reactor outlet, after fitting the steady-state model to industrial data, are presented in parity diagrams for the estimation and cross-validation data in Figure 5. Considering the large period of time used for parameter estimation, the model shows good agreement with the industrial data, as well as the capability of predicting the product distribution.

Figure 6 shows that the proposed model can predict the trends of the temperatures in the reactor and regenerator with the changes in the operating conditions, showing relative errors not higher than 2.2% in the predicted temperatures (Table 6) and a mean relative error lower than 1%.

It is important to note that there are always errors associated to the temperature sensors, and while the model considers homogeneous average temperatures in the regenerator and reactor vessel volumes, this is not entirely true in an industrial unit, since the temperature measured often depends on the sensor locations.[45] This means that there is some degree of uncertainty in the industrial temperatures used for comparison, which easily accounts for the errors found in the comparison above.

More important than predicting the exact values of the temperatures is to predict the variations in the temperatures with the operating variables. Therefore, it is fundamental that the heat balance predicted by the model matches well the heat balance of the industrial unit, since it conditions the behavior of many operating variables. It is widely assumed that a FCC unit produces and burns enough coke to adjust itself in terms of energy needs. The difference between the coke on the spent catalyst and the coke on regenerated catalyst, expressed as weight percent of catalyst, is the unit delta coke, Δcoke:

$$\Delta\text{coke} = Y_{\text{ck,RT}} - Y_{\text{ck,RG}} = \frac{\text{CK yield (wt \% feed)}}{\text{COR (kg/kg)}} \quad (12)$$

The delta coke influences directly the temperatures in the FCC unit; for a particular case with approximately constant

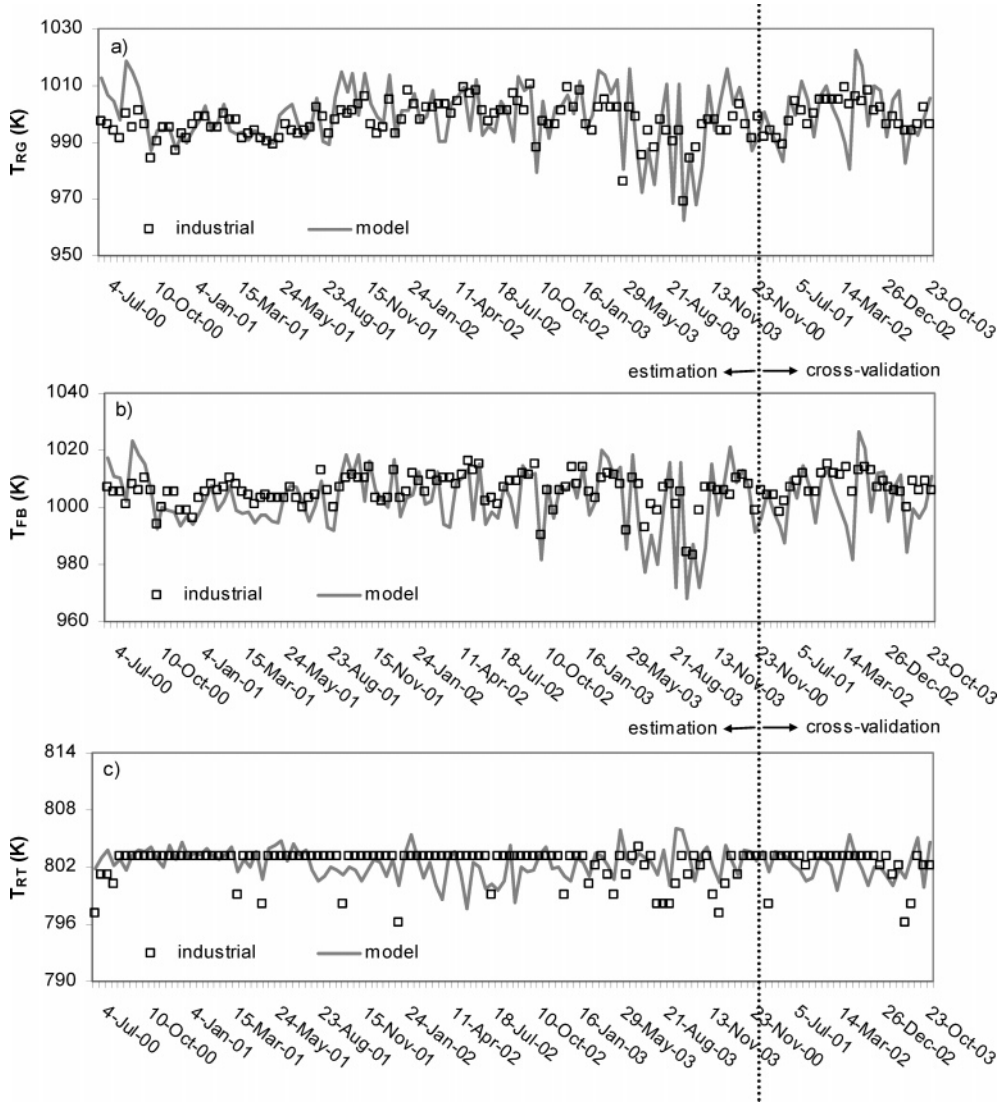

Figure 6. Industrial and model predicted temperatures for the estimation and cross-validation data sets: (a) regenerator vessel dense bed, (b) regenerator vessel freeboard, (c) riser reactor.

Table 6. Mean and Maximum Relative Errors in the Model Predictions for the Riser Reactor and Regenerator Temperatures

process variable	mean error (%)	maximum error (%)
riser reactor temperature, T_{RT} (K)	0.19%	0.7%
regenerator bed temperature, T_{RG} (K)	0.63%	2.2%
regenerator freeboard temperature, T_{FB} (K)	0.63%	2.8%

catalyst heat capacity and coke's specific heat of combustion, for constant H/C in the coke and identical degree of CO combustion, the delta coke is expected to be proportional to the temperature difference between the regenerator and the reactor. Figure 7a shows that this proportionality holds both for the industrial unit as well as for the model. The dispersion found is due to the variation in the H/C in coke in the studied cases. Figure 7b also shows good agreement between the model predictions and the industrial data, with variations of the catalyst-to-oil ratio (COR) and coke yield as expected.[37]

5. Simulation Studies

After regression of the model parameters, it is now possible to study the behavior of the unit, to verify if the model shows a consistent behavior with what is typically observed, in a wider range of operation. This study was done using standard industrial operating conditions, as well as a typical VGO feedstock and equilibrium catalyst. All the necessary inputs are listed in Tables 3 and 7. Additional data, concerning unit dimensions, thermodynamic data, and combustion kinetic parameters, are given in Appendix A2.

5.1. Steady-State Behavior. Figure 8 shows the influence of the catalyst-to-oil ratio (COR) in the reactor and regenerator temperatures and in the product yields and conversion. It is observed that increasing the COR leads to an increase in the riser outlet temperature (Figure 8a, T_{RT}), since a higher COR means that there is more catalyst available for the same quantity of hydrocarbons. For the same reason, a higher COR will also contribute to a higher conversion of the feed (lower VGO yield), as can be seen in Figure 8b. Although there is an increase in coke yield (Figure 8b, CK), the increase in COR leads to a lower coke content on the spent catalyst (Figure 8c, $Y_{ck,ST}$). This decrease in catalyst coke content leads to a lower regenerator temperature (Figure 8a, T_{RG}). These evolutions of temperatures with COR are in agreement with the results presented by other authors.[6] Moreover, in a previous work[1] on the modeling of a R2R unit, this same behavior was also observed. On the other hand, in our recent paper on state multiplicity in a high-efficiency regenerator unit,[12] a curve with a maximum for the

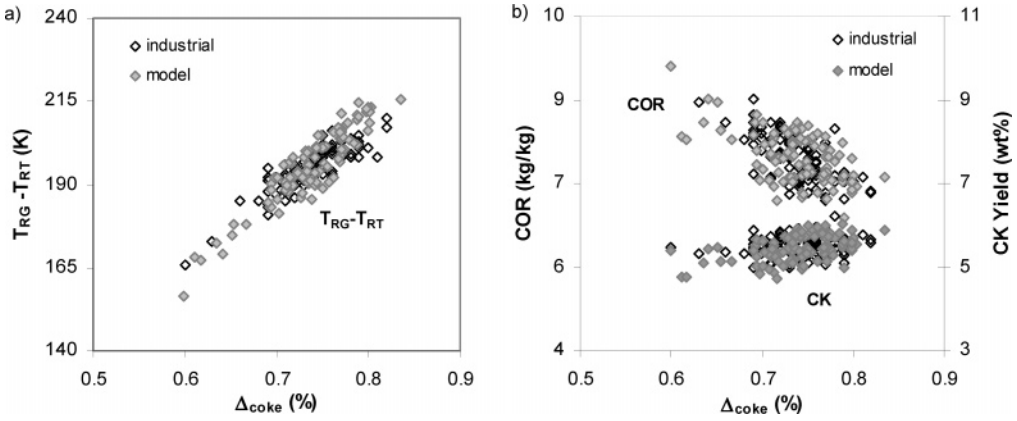

Figure 7. Influence of delta coke on FCC operation: (a) regenerator dense bed temperature, (b) catalyst-to-oil ratio, and coke yield.

Table 7. Feedstock and Catalyst Properties

feedstock property	value
°API gravity, API (deg)	21.05
Watson characterization factor, K_W	11.85
sulfur content, S (wt %)	1.61
Conradson carbon residue, CCR (wt %)	0.79
fraction of CCR converted in coke, x_{CCR}	0.43
catalyst property	**value**
nickel content, Ni (ppm)	930
vanadium content, V (ppm)	1865
average particle diameter, d_p (m)	7.5×10^{-5}
density, ρ_c (kg/m^3)	1382

regenerator profile was obtained. This behavior was also observed by some other authors,[9,46] when there is a transition from partial- to full-combustion mode in the operation range. After model validation, it is clear that the high-efficiency regenerator unit always operates in full-combustion mode, as can be seen in Figure 8d (CO_2/CO). The main differences observed between the simulated behavior before[12] and after validation are due to different coke formation rates and to the use of correlations to predict H/C and ΔH_{crk} in the validated model, which were fixed values before validation.[12]

The effects of COR on VGO conversion and product yields presented in Figure 8b are also consistent with experimental observations[37] and with what other authors reported.[1,6,46] Higher temperatures promote higher conversion rates, mainly in light product yields (LPG and FG), while heavier products like LCO show a slight decrease; after a first increase, GLN goes through a maximum and then starts to decrease.

To further investigate the differences between the model before and after validation, a plot for the influence of air-to-oil ratio in the temperatures and in the flue gas composition at the regenerator dense bed outlet is presented in Figure 9. The reactor and regenerator temperature profiles obtained after model validation are similar to the ones previously obtained before validation. Therefore, a curve with a maximum was obtained for both temperatures (Figure 9a). Moreover, the oxygen concentration and CO_2/CO molar ratio profiles (Figure 9b) after validation are similar to the ones obtained before validation.[12]

The profiles along the axial coordinate in the riser were also investigated and are presented in Figure 10, for some process variables. These results are very similar to the ones obtained by Fernandes et al.,[1] since the riser model is the same, and are in agreement with what was observed by other authors.[6,9,46]

Figure 10a shows that the temperature decreases significantly along the riser, which is expected since the cracking reactions are highly endothermic. Along with the temperature, the pressure also decreases (Figure 10c). However the pressure drop in the riser is not as significant as the temperature decrease, since there is a molar expansion of about 4 times the total number of moles in the gas phase that slows down the pressure decrease. This molar expansion is responsible for both the increase of gas and solids velocities along the riser and the solids volume fraction decrease, while the gas volume fraction increases as expected (Figure 10b).

Figure 10d shows an initial fast increase in product yields and conversion, which means that most of the cracking reactions occur in the first zone of the riser. This is an expected result because the highest temperatures and lowest coke-on-catalyst content are found at the riser inlet.

5.2. Dynamic Behavior. To study the dynamic behavior of the FCC model here presented, dynamic simulations were done for typical disturbances to the FCC unit. The open-loop dynamic responses of the system to perturbations in the feed flow rate and in the combustion air flow rate will then be presented and discussed. Figure 11 shows the dynamic response of the system to step perturbations in the gas oil feed rate of −3% at 1 000 s and 3% at 10 000 s (Figure 11a, $F_{HC,FF}$).

Decreasing the fresh feed flow rate initially results in a small decrease of the spent catalyst flow (Figure 11c, $F_{c,RT}$), since a lower concentration of hydrocarbons leads to a pressure decrease in the stripper/reactor (Figure 11e, P_{RT}). On the other hand, the pressure decrease in the stripper/reactor causes an increase in the regenerated catalyst flow rate (Figure 11c, $F_{c,RG}$). Since more regenerated catalyst is entering the riser, this means that the COR has increased, which causes an increase in the riser reactor temperature (Figure 11d, T_{RT}). This immediately leads to a steep increase in conversion and an increase in the coke yield (Figure 11b, CK). Although the coke yield has increased, the decrease in the feed flow rate means that a lower quantity of coke can be produced, so the percentage of coke on the spent catalyst decreases (Figure 11c, $Y_{ck,RT}$). With a lower quantity of coke to be burned, the regenerator temperature decreases (Figure 11d, T_{RG}) as well as the production of flue gases. Then again, these two effects cause a decrease in the regenerator pressure (Figure 11e, P_{RG}). The decrease in the regenerator temperature will cause a decrease in the riser reactor temperature, after its initial increase, but not below its initial value.

The evolution to the new steady state is achieved through a pressure balance compensation caused by a decrease of the catalyst level in the regenerator (Figure 11f, L_{RG}) and an increase of the stripper/reactor catalyst level (Figure 11f, L_{RT}). The second perturbation sets the fresh feed flow rate back to its initial value. All the process variables return to their initial steady state.

Although other works that present open-loop dynamic simulations to feed flow rate perturbations can be found in the

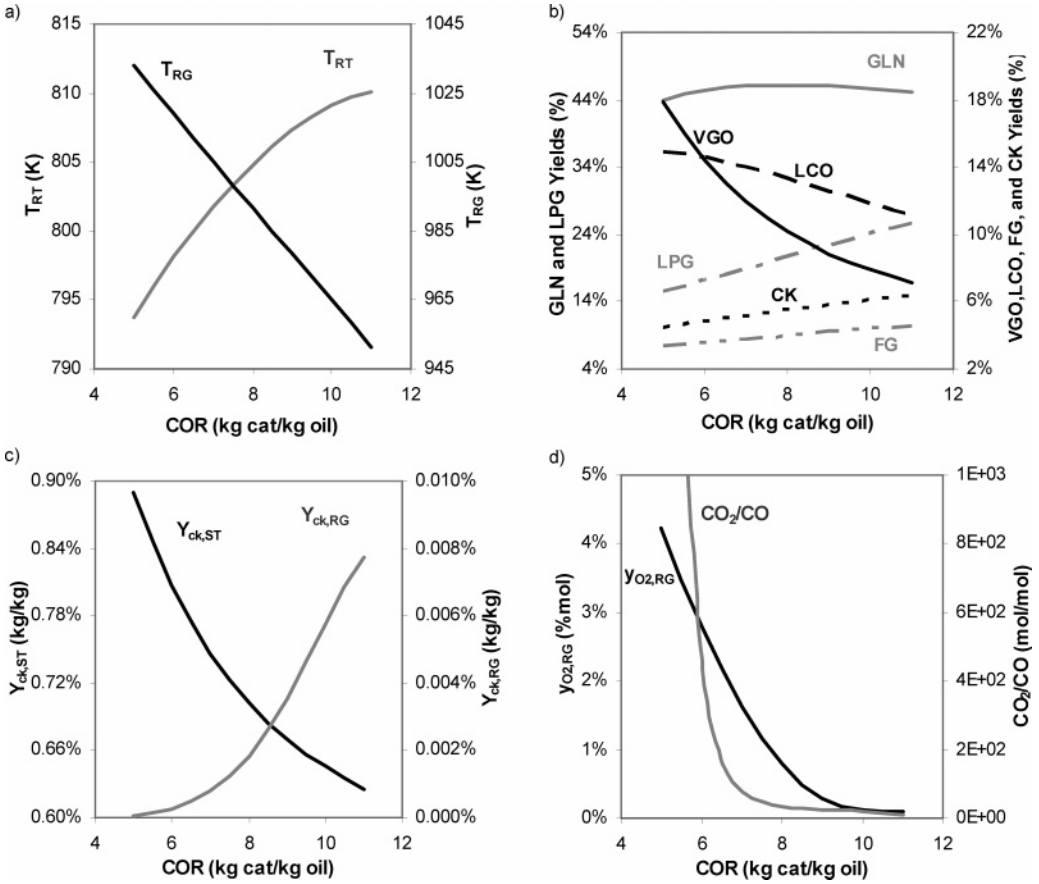

Figure 8. Effect of COR on process variables: (a) reactor and regenerator temperatures, (b) product yields, (c) coke on spent and regenerated catalyst, (d) oxygen molar fraction and CO_2/CO molar ratio in the regenerator.

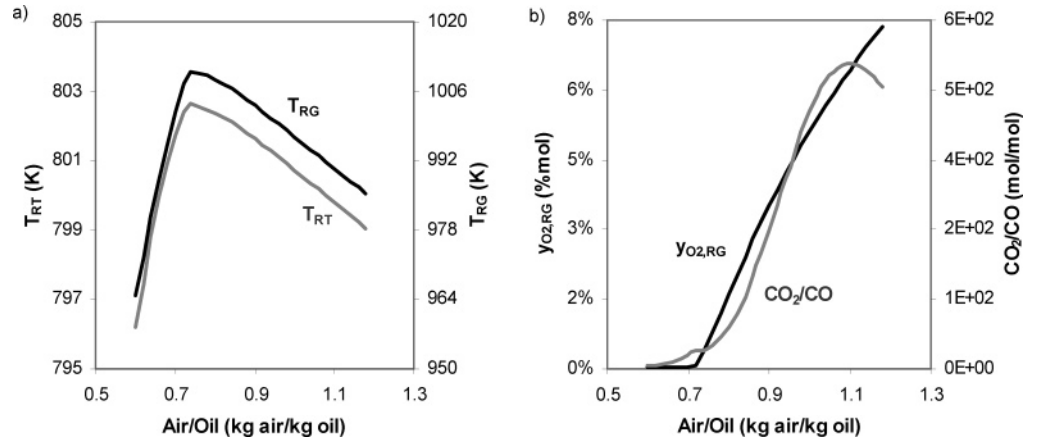

Figure 9. Effect of air/oil on process variables: (a) reactor and regenerator temperatures and (b) oxygen molar fraction and CO_2/CO molar ratio in the regenerator.

literature, direct comparisons with these results cannot be done, since they do not correspond to FCC units with high-efficiency regenerators. However, typical behaviors of FCC units to disturbances can be discussed. It can be seen, for example, that the initial increase in the riser reactor temperature caused by the sudden drop in feed flow rate is a typical behavior also found by other authors[8,46] and in our previous work on the R2R modeling.[1] After this initial rise, there are authors that predict a decrease in the temperature to a lower value than the initial one,[1,8] while others do not predict a decrease at all.[46] In our present work, after the initial increase, the temperature in the riser reactor decreases to a new value that is higher than the initial one.

Other qualitative differences in the transient response to feed flow rate perturbations of this system and of the R2R unit[1] are as follows: (i) the characteristic time of the system, with the high-efficiency regenerator unit showing a much faster response (mainly due to slow kinetics of coke combustion in the regenerator 1 vessel of the R2R); (ii) the initial rise in regenerator temperature is not observed in this system; and (iii) the process gains are lower, which means that the differences between the new steady state and the original one are smaller for this system. On the other hand, the behavior of important process variables such as conversion, coke yield, catalyst flow rates, and catalyst holdups (catalyst bed level) were found to be similar.

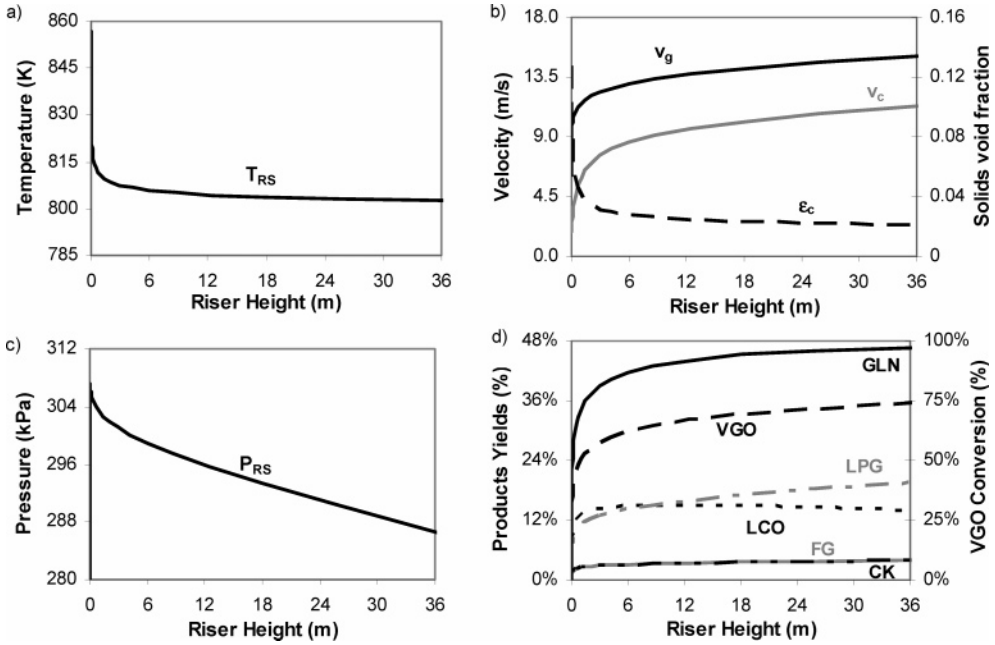

Figure 10. Steady-state profiles along the axial coordinate in the riser: (a) temperature, (b) velocities and solids volume fraction, (c) pressure, and (d) product yields and VGO conversion.

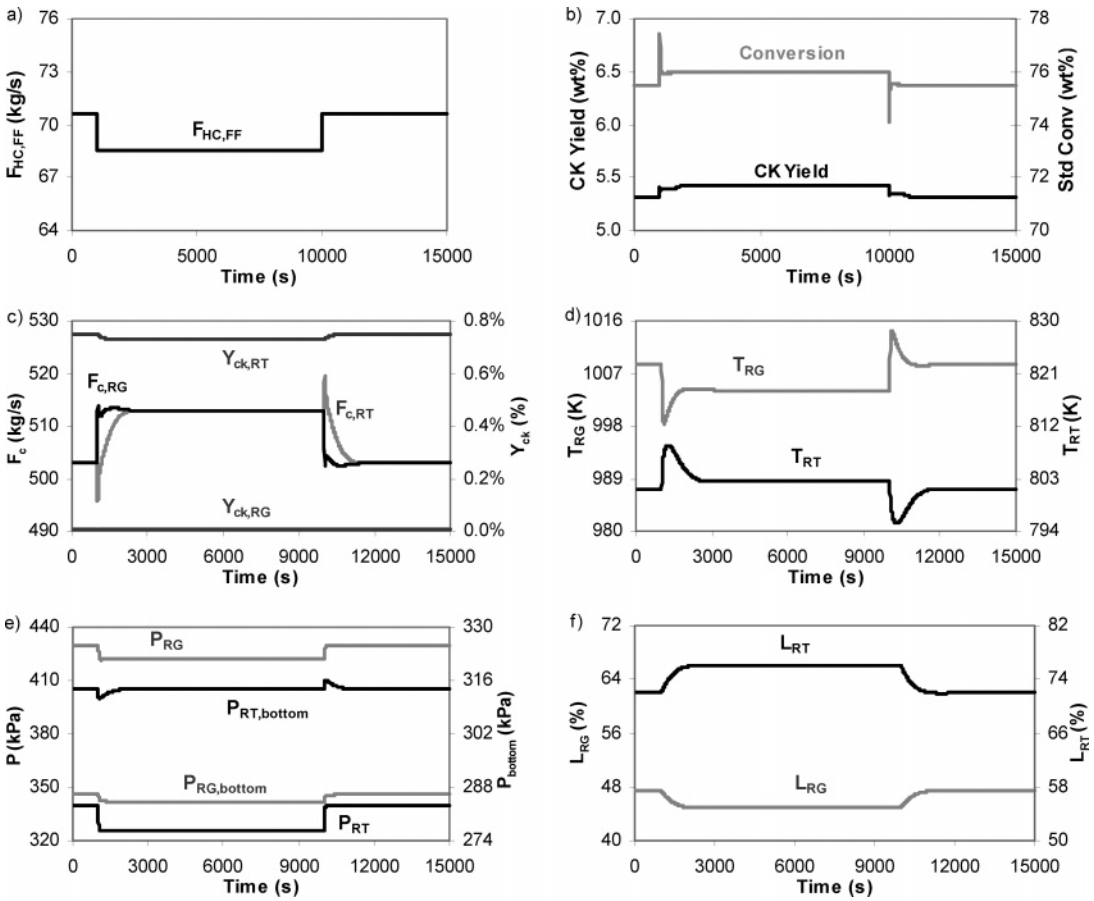

Figure 11. Open-loop simulation for a step perturbation in the feed oil flow rate of −3% at 1 000 s and +3% at 10 000 s: (a) feed flow rate, (b) standard mass conversion and coke yield, (c) spent and regenerated catalyst flow rates and coke content, (d) riser reactor and regenerator temperatures, (e) riser reactor and regenerator pressures, and (f) reactor/stripper and regenerator catalyst bed levels.

A perturbation on the air combustion flow rate was also performed, and the dynamic response of some of the process variables is presented in Figure 12. The step decrease of the combustion air flow rate causes a decrease in the regenerator pressure (Figure 12e, P_{RG}). On the other hand, the lower pressure causes a decrease in the catalyst flow rate (Figure 12c, $F_{c,RG}$) and, consequently, a decrease in the riser reactor temperature (Figure 12d, T_{RT}) and conversion (Figure 12b). The temperature in the regenerator initially rises (Figure 12d, T_{RG}), because of a lower dilution effect caused by a lower quantity of air (this happens only in excess oxygen conditions); however, since the temperature in the riser reactor decreased and the coke

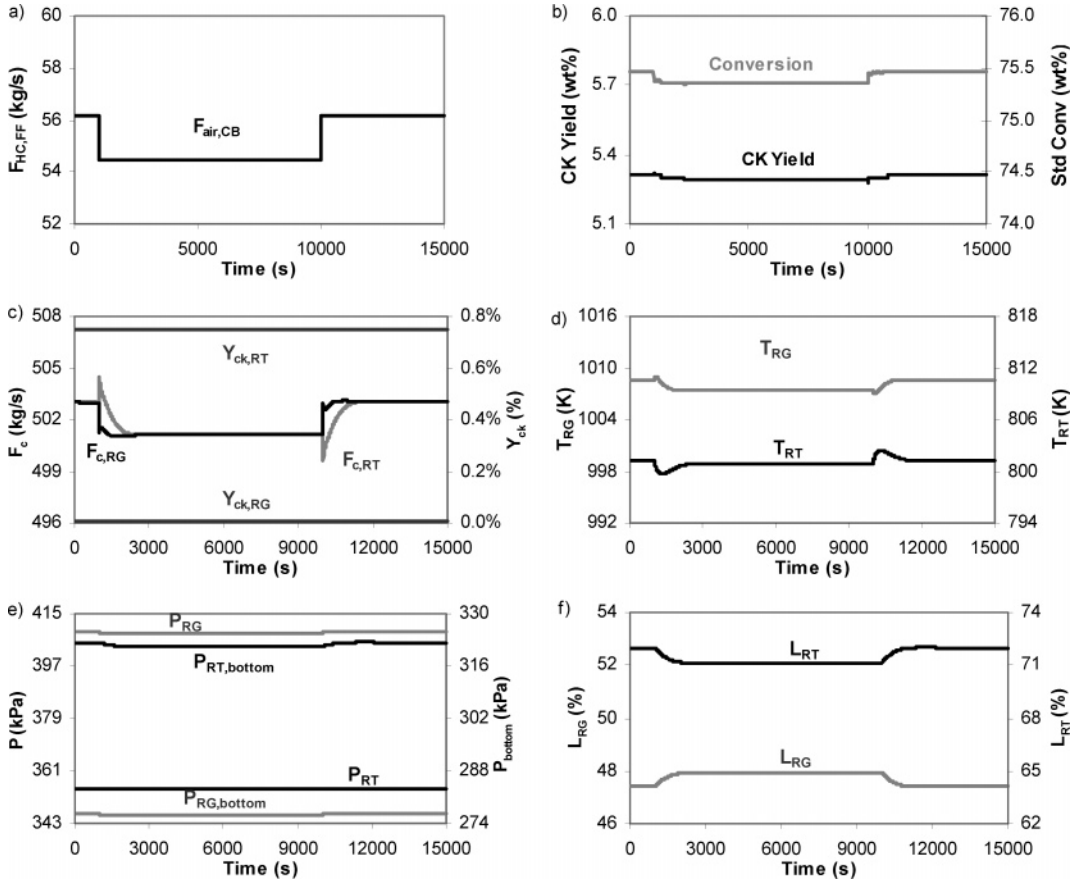

Figure 12. Open-loop simulation for a step perturbation in the combustion air flow rate of −3% at 1 000 s and +3% at 10 000 s: (a) feed flow rate, (b) standard mass conversion and coke yield, (c) spent and regenerated catalyst flow rates and coke content, (d) riser reactor and regenerator temperatures, (e) riser reactor and regenerator pressures, and (f) reactor/stripper and regenerator catalyst bed levels.

concentration on the spent catalyst remains nearly constant (Figure 12c, $Y_{ck,RT}$), the regenerator temperature decreases after its initial rise. To balance the pressure decrease in the regenerator, the catalyst holdup in the stripper will decrease (Figure 12f, L_{RT}), while the bed level in the regenerator will increase (Figure 12f, L_{RG}). Increasing the combustion air flow rate to its initial value will lead the system to the initial steady state.

Again, even though a direct comparison cannot be established, the observed decrease in temperatures and conversion with the decrease of combustion air flow rate is in good agreement with the results presented by Arandes and De Lasa.[7] From Figures 11 and 12, it is also clear that disturbances in the feed flow rate affect much more significantly the system than disturbances in the air flow rate. This had already been observed for the R2R unit.[1] On the other hand, there are some differences in the transient response to air perturbations between these two units. This is expected, since these two units have different regenerator configurations and the perturbed variable is directly connected to the regeneration system. Therefore, in the high-efficiency regenerator, the regenerator temperature does not show a steep decrease after the perturbation occurred; the reactor temperature decreases immediately after the perturbation, and consequently, the conversion also decreases without showing the initial steep increase found for the R2R unit. Once again, the response time is much smaller for the high-efficiency regenerator unit, and the catalyst flow rates, the catalyst holdups, and the pressures in the reactor and regenerator vessels show similar behaviors.

6. Conclusions

A simulator for an industrial fluid catalytic cracking (FCC) UOP unit with a high-efficiency regenerator was developed, which implements a detailed mathematical model in FORTRAN. This simulator can predict both the steady-state and the dynamic state of an industrial FCC unit with a high-efficiency regenerator.

The steady-state model was validated with industrial routinely available data from a period of 3.5 years. In order to predict the major classes of cracking products of a real operating FCC UOP unit, some correlations that are a function of feedstock and equilibrium catalyst properties were included in the kinetic model. A set of parameters was estimated by fitting the model predictions to routinely available industrial data. All of the parameters estimated present statistical confidence for an interval of 95%.

The model obtained showed a consistent behavior with what is usually observed in a FCC unit, both for steady-state and dynamic open-loop simulations. Thus, this model is well-suited to be used as a reference model in studies of advanced control and real-time optimization.

Acknowledgment

J.L.F. thanks the financial support granted by the program POCTI—Formar e Qualificar from Fundação para a Ciência e Tecnologia through Grant No. SFRH/BD/12853/2003 and Galpenergia ARL for the supply of industrial data.

Appendix

A1. Regenerator Vessel Model Equations. Equations A1−A5 present the overall mass balances done to the regenerator vessel to determine the pressure and catalyst level in the vessel.

Catalyst inventory:

$$\frac{\partial W_{c,RG}}{\partial t} = F_{c,LF} - F_{c,RG} - F_{rc,RG} \tag{A1}$$

Catalyst bed level:

$$L_{RG} = \frac{W_{c,RG}}{\rho_c \epsilon_{c,RG} \Omega_{RG}} \tag{A2}$$

Gas inventory:

$$\frac{\partial W_{g,RG}}{\partial t} = F_{g,LF} + F_{air,RG} - F_{g,RG} + \sum_i F_{c,LF} Y_{i,LF} - \sum_i (F_{c,RG} + F_{rc,RG}) Y_{i,RG} \tag{A3}$$

Pressure balance:

$$P_{RG} = W_{g,RG} \frac{RT_{RG}}{\bar{M}^g_{w,RG} V_{g,RG}} \tag{A4}$$

$$P_{RG_{bottom}} = P_{RG} + \rho_c (1 - \epsilon_{bed}) L_{RG} g \tag{A5}$$

The mass balances to the species and the energy balance were done separately for the freeboard and dense bed regions in the regenerator vessel. Equations A6−A8 are the balances in the dense bed, while eqs A9−A12 are the balances in the freeboard region.

A1.1. Dense Bed.

Gaseous species molar balance:

$$V_{bed} \frac{\partial C_{i,RG}}{\partial t} = N^g_{i,LF} + N^{air}_{i,RG} - N^g_{i,RG} + V_{bed}(\epsilon_{g,RG} \sum_j (r^g_j \upsilon^g_{ji}) + \epsilon_{c,RG} \rho_c \sum_j (r^s_j \upsilon^s_{ji})) \tag{A6}$$

Carbon and hydrogen mass balance:

$$\frac{W_{c,RG}}{M_{w,i}} \frac{\partial Y_{i,RG}}{\partial t} = \frac{F_{c,LF}}{M_{w,i}} Y_{i,LF} - \frac{F_{c,RG} + F_{rc,RG}}{M_{w,i}} Y_{i,RG} + V_{bed} \epsilon_{c,RG} \rho_c \sum_j (r^s_j \upsilon^s_{ji}), \quad i = \text{C or H} \tag{A7}$$

Energy balance:

$$\frac{\partial (W_{c,RG} C_{Pc} T_{RG} + W_{g,RG} C_{Pg} T_{RG})}{\partial t} = F_{g,LF} H_{g,LF} + F_{c,LF} H_{c,LF} + Y_{ck,LF} F_{c,LF} H_{ck,LF} + F_{air,RG} H_{air,RG} - Y_{ck,RG} (F_{c,RG} + F_{rc,RG}) H_{ck,RG} - F_{g,RG} H_{g,RG} - (F_{c,RG} + F_{rc,RG}) H_{c,RG} + Q^\circ_r + Q_{loss} \tag{A8}$$

A1.2. Freeboard.

Gaseous species molar balance:

$$\frac{\partial N^g_{i,FB}}{\partial z} = \Omega_{FB} \sum_j (r^g_j \upsilon^g_{ji}) \qquad i = N_2, O_2, CO, CO_2, \text{ and } H_2O \tag{A9}$$

$$N^g_{N_2,FB}|_{z=0} = N^g_{N_2,RG}, \quad N^g_{O_2,FB}|_{z=0} = N^g_{O_2,RG}, \quad N^g_{CO,FB}|_{z=0} = N^g_{CO,RG}, \quad N^g_{CO_2,FB}|_{z=0} = N^g_{CO_2,RG}, \quad N^g_{H_2O,FB}|_{z=0} = N^g_{H_2O,RG} \tag{A10}$$

Energy balance:

$$\sum_i F_{i,FB} C_{p_i} \frac{\partial T_{FB}}{\partial z} = -\Omega_{FB} \sum_j (r^g_j \Delta H^g_j) + \pi D_{FB} U_{FB} (T_{surr} - T_{FB}) \tag{A11}$$

$$T_{FB}|_{z=0} = T_{RG} \tag{A12}$$

Equations A13−A27 represent additional relations needed to solve the mass and energy balances presented above.

$$F_{g,RG} = k_{v,RG} f(x_v) \sqrt{P_{RG} - P_{SG}} \tag{A13}$$

$$V_{g,RG} = V_{RG} - \frac{W_{c,RG}}{\rho_c} \tag{A14}$$

$$\bar{M}^g_{w,RG} = \sum_i y_{i,RG} M_{w,i} \qquad i = N_2, O_2, CO, CO_2, \text{ and } H_2O \tag{A15}$$

$$y_{i,RG} = \frac{C_{i,RG}}{\sum_i C_{i,RG}} \qquad i = N_2, O_2, CO, CO_2, \text{ and } H_2O \tag{A16}$$

$$N^{air}_{i,RG} = \frac{F_{air,RG}}{M_{w,i}} w^{air}_{i,RG} \qquad i = N_2, O_2, CO, CO_2, \text{ and } H_2O \tag{A17}$$

$$N^g_{i,RG} = y_{i,RG} \frac{F_{g,RG}}{\bar{M}^g_{w,RG}} \qquad i = N_2, O_2, CO, CO_2, \text{ and } H_2O \tag{A18}$$

The bed voidage in the dense bed of the regenerator vessel is given by the correlation proposed by King:[47]

$$\epsilon_{g,RG} = \frac{u_g + 1}{u_g + 2} \tag{A19}$$

$$\epsilon_c = 1 - \epsilon_g \tag{A20}$$

$$u_{g,RG} = \frac{F_{g,RG}}{\rho_{g,RG} \Omega_{RG}} \tag{A21}$$

$$\rho_{g,RG} = \frac{P_{RG} \bar{M}^g_{w,RG}}{RT_{RG}} \tag{A22}$$

$$V_{bed} = L_{RG} \Omega_{RG} \tag{A23}$$

$$Y_{ck,RG} = Y_{C,RG} + Y_{H,RG} \tag{A24}$$

$$H_k = C_{pk} (T_k - T_{ref}) \qquad k = \text{c, CK, and g} \tag{A25}$$

$$Q^\circ_r = V_{bed} (\epsilon_{g,RG} \sum_j r^g_j \Delta H^g_j + \epsilon_{c,RG} \rho_c \sum_j r^s_j \Delta H^s_j) \tag{A26}$$

$$Q_{loss} = \pi D_{RG} L_{RG} U_{RG} (T_{surr} - T_{RG}) \tag{A27}$$

A2. Additional Data for Simulation. In Tables A1−A5, additional data necessary for the simulations presented in this study are given. These values concern the approximate real dimensions of the FCC unit; the valve flow rating

Table A1. UOP FCC Unit Dimensions

UOP FCC unit dimensions	length (m)	diameter (m)
riser	37.11	1.39
stripper	12.44	3.56
disengager	7.80	6.66
combustor	7.4	6.09
lift	10.7	2.5
regenerator	13.7	9.3
spent catalyst standpipe	10.9	0.86
recirculated regenerated catalyst standpipe	4.65	0.86
regenerated catalyst standpipe	9.35	0.86

Table A2. Valves Flow Rating Characteristic Factors and Functions

valve	characteristic constant, k_v (kg/(s·Pa$^{0.5}$))
main fractionator, $k_{v,MF}$	0.19
spent catalyst slide valve, $k_{v,SCSV}$	3.01
regenerated catalyst slide valve, $k_{v,RCSV}$	5.27
regenerated catalyst slide valve, $k_{v,RCRSV}$	12.22
flue gas valve, $k_{v,FG}$	0.21
flue gas valve characteristic function, $f(x_v)$	$f(x_v) = (x_v)/(\sqrt{0.07 + (1 - 0.07)x_v^2})$

Table A3. Average Molecular Weights of the Lumps in the Kinetic Model

lump	molecular weight (g/mol)
vacuum gas oil, VGO	400
light cycle oil, LCO	200
gasoline, GLN	100
liquefied petroleum gases, LPG	50
fuel gas, FG	25
coke, CK	400

Table A4. Thermodynamic Properties for Feedstock, Equilibrium Catalyst, and Combustion Gases

Feedstock, Catalyst and Unit Properties	
specific heat, C_{pHC} (J/(kg·K))	1255.5
specific heat, C_{pc} (J/(kg·K))	1197.5
overall heat coefficient, U (J/(m^2·s·K))	40
Heats of Formation[47]	
coke, $\Delta H_f(CH_x)$ (J/mol)	$-4800.22 + 16.1T$
oxygen, $\Delta H_f(O_2)$ (J/mol)	$-10364.88 + 34.60T + 0.00055T^2$
carbon monoxide, $\Delta H_f(CO)$ (J/mol)	$-118975.04 + 27.61T + 0.00251T^2$
carbon dioxide, $\Delta H_f(CO_2)$ (J/mol)	$-406909.11 + 43.26T + 0.00575T^2$
water, $\Delta H_f(H_2O)$ (J/mol)	$-252111.38 + 34.39T + 0.00031T^2$

Table A5. Kinetic Model for Coke Combustion Reactions[1]

carbon combustion	
k_{C1}^{dry} (s^{-1}·Pa$^{-0.78}$)	$9.45 \times 10^2 \exp(-1.43 \times 10^5/RT)$
k_{C1}^{wet} (Pa$^{0.11}$)	$2.35 \times 10^4 \exp(-7.92 \times 10^4/RT)$
k_{C2}^{dry} (s^{-1}·Pa^{-1})	$7.23 \times 10^1 \exp(-1.59 \times 10^4/RT)$
k_{C2}^{wet} (Pa$^{-0.16}$)	$5.10 \times 10^5 \exp(-1.77 \times 10^4/RT)$
k_{C3}^{wet} (s^{-1}·Pa$^{-0.1}$)	$1.21 \times 10^3 \exp(-2.71 \times 10^4/RT)$
$f(X_C)$	$3.0X_C^3 - 2.5X_C^2 + X_C + 0.7$
hydrogen combustion: k_3^s (mol·s^{-1}·kg^{-1}·cat)	$4.03 \times 10^6 \exp(-1.58 \times 10^5/RT)$
heterogeneous CO oxidation: k_4^s (mol·s^{-1}·kg^{-1}·cat)	$3.89 \times 10^{-6} \exp(-1.15 \times 10^4/RT)$
homogeneous CO oxidation: k_1^g (mol·s^{-1}·m^{-3})	$8.45 \times 10^{22} \exp(-2.53 \times 10^5/RT)$

factors; the average molecular weights of the kinetic lumps; the thermodynamic properties of the feedstock, equilibrium catalyst, and combustion gases; and the coke combustion kinetics.

The average molecular weights of the kinetic lumps are the same as the ones proposed by Pitault et al.[17] The kinetic model for coke combustion is presented in detail by Fernandes et al.[1]

Nomenclature

Symbols

a_{ij} = cracking kinetic parameter of the reaction lump $i \rightarrow$ lump j
A_{ij} = cracking kinetic constant of the reaction lump $i \rightarrow$ lump j (s^{-1} or $m^3/(s \cdot kg)$)
°API = °API density parameter
b_{ij} = cracking kinetic parameter of the reaction lump $i \rightarrow$ lump j
c_i = cracking kinetic parameter for the formation of lump i
C_p = specific heat capacity (J/(kg·K))
CCR = Conradson carbon residue in the feed (wt %)
d = deactivation order
E_{ij} = activation energy of the reaction lump $i \rightarrow$ lump j (J/mol)
F = mass flow rate (kg/s)
H/C = hydrogen-to-carbon molar ratio
k_v = valve flow rating factor kg/(s·kPa$^{0.5}$)
k = rate coefficient of the combustion reactions
K_W = Watson characterization factor
M_{MI} = Mobil metal index (ppm)
M_w = molar mass (kg/mol)
Ni = nickel content in the equilibrium catalyst (ppm)
n_{ij} = order of the reaction lump $i \rightarrow$ lump j
P = pressure (Pa)
r_{ij} = rate of the reaction lump $i \rightarrow$ lump j (kg/(m^3·s))
R = universal gas constant (J/(mol·K))
S = sulfur content in the feedstock (wt %)
T = temperature (K)
U = overall heat transfer coefficient (J/(m^2·s·K))
v = velocity (m/s)
V = vanadium content on equilibrium catalyst (ppm)
w = mass fraction (wt %)
x_{CCR} = fraction of CCR that converts to coke
X_C = carbon conversion of the coke (kg/kg)
x_v = valve opening, [0−1]
Y_{ck}^{cat} = catalytic coke content of catalyst ((kg of catalytic coke)/(kg of catalyst))
Y_{ck} = total coke content of catalyst ((kg of coke)/(kg of catalyst))

Greek Letters

α = deactivation constant ((kg of catalyst)/(kg of catalytic coke))
α_v = valve constant parameter, [0−1]
Δcoke = delta coke (%)
ΔH_{crk} = heat of cracking per unit mass of VGO converted (J/kg)
ΔH_f = heat of formation (J/mol)
ϵ = volume fraction (m^3/m^3)
Φ = catalyst deactivation function
θ_{SP} = angle of inclination of the standpipe (deg)
ρ = density (kg/m^3)

Subscripts, Superscripts, and Abbreviations

CB = combustor section
CK = coke

COR = catalyst-to-oil ratio
c = catalyst
dry = refers to dry conditions in the regenerator
FB = freeboard section
FCC = fluid catalytic cracking
FF = fresh feed
FG = fuel gas
FV = feed vaporization section
GLN = gasoline
g = gas
HC = hydrocarbons
i, *j* = lump or gaseous species
LCO = light cycle oil
LF = lift section
LPG = liquefied petroleum gases
MF = main fractionator
p = catalyst particle
rc = recirculated catalyst
RCSV = regenerated catalyst slide valve
RCRSV = recirculated catalyst slide valve
RG = regenerator section
RS = riser section
RT = reactor (includes riser and disengager/stripper sections)
SG = stack gases (=flue gases) or specific gravity
SP = standpipes section
SP_R = regenerated catalyst standpipe
SP_S = spent catalyst standpipe
ST = disengager/stripper section
s = solids
surr = surroundings
VGO = vacuum gas oil
wet = refers to wet conditions in the regenerator

Literature Cited

(1) Fernandes, J. L.; Verstraete, J.; Pinheiro, C. I. C.; Oliveira, N. M. C.; Ribeiro, F. R. Dynamic modelling of an industrial R2R FCC unit. *Chem. Eng. Sci.* **2007**, *62*, 1184.

(2) Secchi, A. R.; Santos, M. G.; Neumann, G. A.; Trierweiler, J. O. A Dynamic Model for a FCC UOP Stacked Converter Unit. *Comput. Chem. Eng.* **2001**, *25* (4−6), 851.

(3) Moro, L. F. L.; Odloak, D. Constrained multivariable control of fluid catalytic cracking converters. *J. Process Control* **1995**, *5* (1), 29.

(4) Elnashaie, S. S. E. H.; Mohamed, N. F.; Kamal, M. Simulation and Static Bifurcation Behavior of Industrial FCC Units. *Chem. Eng. Commun.* **2004**, *191*, 813.

(5) Ansari, R. M.; Tadé, M. O. Constrained nonlinear multivariable control of a fluid catalytic cracking process. *J. Process Control* **2000**, *10*, 539.

(6) Malay, P.; Milne, B. J.; Rohani, S. The Modified Dynamic Model of a Riser Type Fluid Catalytic Cracking Unit. *Can. J. Chem. Eng.* **1999**, *77* (February), 169.

(7) Arandes, J. M.; De Lasa, H. I. Simulation and Multiplicity of Steady States in Fluidized FCCUs. *Chem. Eng. Sci.* **1992**, *47*, 2535.

(8) McFarlane, R. C.; Reineman, R. C.; Bartee, J. F.; Georgakis, C. Dynamic Simulator for a Model IV Fluid Catalytic Cracking Unit. *Comput. Chem. Eng.* **1993**, *17* (3), 275.

(9) Arbel, A.; Huang, Z.; Rinard, I. H.; Shinnar, R. Dynamic and Control of Fluidized Catalytic Crackers. 1. Modeling of the Current Generation of FCC's. *Ind. Eng. Chem. Res.* **1995**, *34*, 1228.

(10) Han, I.-S.; Chung, C.-B. Dynamic modeling and simulation of a fluidized catalytic cracking process. Part I: Process modeling. *Chem. Eng. Sci*. **2001**, *56*, 1951.

(11) Ali, H. K. A.; Rohani, S. Dynamic Modelling and Simulation of a Riser Type Fluid Catalytic Cracking Unit. *Chem. Eng. Technol*. **1997**, *20* (2), 118.

(12) Fernandes, J. L.; Pinheiro, C. I. C.; Oliveira, N. M. C.; Neto, A. I.; Ribeiro, F. R. Steady state multiplicity in a UOP FCC unit with a high-efficiency regenerator. *Chem. Eng. Sci*. **2007**, *62*, 6308.

(13) Corella, J.; García-Dopico, M.; Francés, E. An advanced model for a whole FCCU based on the kinetics and on basic principles. Part I: The model in detail. In *Recent Advances in FCC Technology Symposium*, AIChE Spring Meeting, April 17−21, 1994, Atlanta, GA.

(14) Weekman, V. W. A model of catalytic cracking conversion in fixed, moving and fluid-bed reactors. *Ind. Eng. Chem. Process Des. Dev.* **1968**, *7*, 90.

(15) Jacob, S.; Gross, B.; Voltz, S. E.; Weekman, V. W. A Lumping and Reaction Scheme for Catalytic Cracking. *AIChE J*. **1976**, *22*, 701.

(16) Takatsuka, T.; Sato, S.; Morimoto, Y.; Hashimoto, H. A Reaction Model for Fluidized-Bed Catalytic Cracking of Residual Oil. *Int. Chem. Eng*. **1987**, *27*, 107.

(17) Pitault, I.; Nevicato, D.; Forissier, M.; Bernard, J.-R. Kinetic Model based on a Molecular Description for Catalytic Cracking of Vacuum Gas Oil. *Chem. Eng. Sci.* **1994**, *49*, 4249.

(18) Ancheyta-Juárez, J.; López-Isunza, F.; Aguilar-Rodríguez, E. 5-Lump kinetic model for gas oil catalytic cracking. *Appl. Catal., A* **1999**, *177*, 227.

(19) Hagelberg, P.; Eilos, I.; Hiltunen, J.; Lipiäinen, K.; Niemi, V. M.; Aittamaa, J.; Krause, A. O. I. Kinetics of catalytic cracking with short contact times. *Appl. Catal., A* **2002**, *223*, 73.

(20) Gianetto, A.; Farag, H. I.; Blasetti, A. P.; De Lasa, H. I. Fluid Catalytic Cracking Catalyst for Reformulated Gasolines. Kinetic Modeling. *Ind. Eng. Chem. Res.* **1994**, *33*, 3053.

(21) Weekman,V. W.; Nace, D. M. Kinetics of Catalytic Cracking Selectivity in Fixed, Moving, and Fluid Bed Reactors. *AIChE J*. **1970**, *16*, 397.

(22) Corma, A.; Melo, F. A.; Sauvanaud, L. Kinetic and decay cracking model for a MicroDowner unit. *Appl. Catal., A* **2005**, *287*, 34.

(23) Delattre, C.; Forissier, M.; Pitault, I.; Schweich, D.; Bernard, J. R. Improvement of the microactivity test for kinetic and deactivation studies involved in catalytic cracking. *Chem. Eng. Sci.* **2001**, *56*, 1337.

(24) Corella, J.; Frances, E. On the kinetic equation of deactivation of commercial cracking (FCC) catalysts with commercial feedstocks. In *Catalyst Deactivation, 1991*; Bartholomew, C. H., Butt, J. B., Eds.; Elsevier: New York, 1991; p 375.

(25) Farrauto, R. J.; Bartholomew, C. H. *Fundamentals of Industrial Catalytic Processes*; Blackie Academic & Professional: London, 1997.

(26) Wojciechowski, B. W.; Corma, A. Catalytic Cracking. In *Catalysts, Chemistry and Kinetics, Chemical Industries 25*; Marcel Dekker: New York, 1986.

(27) Corella, J.; Bilbao, R.; Molina, J. A.; Artigas, A. Variation with time of the mechanism, observable order, and activation energy of the catalyst deactivation by coke in the FCC process. *Ind. Eng. Chem. Process Des. Dev.* **1985**, *24*, 625.

(28) Froment, G.; Bischoff, K. *Chemical Reactor Analysis and Design, Wiley Series in Chemical Engineering*, 2nd ed.; John Wiley & Sons: New York, 1990.

(29) Nam, I.-S.; Kittrell, J. R. Use of Catalyst Coke Content in Deactivation Modeling. *Ind. Eng. Chem. Process Des. Dev.* **1984**, *23*, 237.

(30) Corella, J.; Monzón, A. Modeling of the deactivation kinetics of solid catalysts by two or more simultaneous and different causes. *Ind. Eng. Chem. Res.* **1988**, *27*, 369.

(31) García-Dopico, M.; García, A.; Santos, García. A. Modelling coke formation and deactivation in a FCCU. *Appl. Catal., A* **2006**, *303*, 245.

(32) De Lasa, H. I.; Grace, J. R. The Influence of the Freeboard Region in a Fluidized Bed Catalytic Cracking Regenerator. *AIChE J*. **1979**, *6* (6), 984.

(33) Brent, R. P. An algorithm with guaranteed convergence for finding a zero of a function. *Comput. J*. **1971**, *14*, 422.

(34) Powell, M. J. D. A hybrid method for nonlinear equations. In *Numerical Methods for Nonlinear Algebraic Equations*; Rabinowitz, P., Ed.; Gordon and Breach: London, 1988.

(35) Li, S.; Petzold, L. *Design of New DASPK for Sensitivity Analysis*; Technical Report; Department of Computer Science, University of California Santa Barbara: Santa Barbara, CA, 1999.

(36) Sadeghbeigi, R. *Fluid Catalytic Cracking Handbook−Design, Operation and Troubleshooting of FCC Facilities*; Gulf Publishing Company: Houston, TX, 2000.

(37) Montgomery, J. *The Grace Davison Guide to Fluid Catalytic Cracking−Part One*; W. R. Grace & Co.-Conn.: Baltimore, MD, 1993.

(38) Montgomery, J. *The Grace Davison Guide to Fluid Catalytic Cracking−Part Two*; W. R. Grace & Co.-Conn.: Baltimore, MD, 1996.

(39) Voltz, S. E.; Nace, D. M.; Weekman, V. W. Application of a Kinetic Model for Catalytic Cracking. Some Correlations of Rate Constants. *Ind. Eng. Chem. Process Des. Dev.* **1971**, *10*, 538.

(40) Ancheyta-Juárez, J.; López-Isunza, F.; Aguillar-Rodríguez, E. Correlations for Predicting the Effect of Feedstock Properties on Catalytic Cracking Kinetic Parameters. *Ind. Eng. Chem. Res.* **1998**, *37*, 4637.

(41) Mitchell, B. R. Metal Contamination of Cracking Catalysts. 1. Synthetic Metals Deposition on Fresh Catalysts. *Ind. Eng. Chem. Prod. Res. Dev.* **1980**, *19* (2), 209.

(42) Leuenberger, E. L. Method Predicts Activity of Vanadium-Contaminated FCC Catalyst. *Oil Gas J.* **1985**, *July 15*, 125.

(43) Larocca, M.; Farag, H.; Ng, S.; De Lasa, H. Cracking Catalyst Deactivation by Nickel and Vanadium Contaminants. *Ind. Eng. Chem. Res.* **1990**, *29*, 2181.

(44) Dennis, J. E.; Gay, D. M.; Welsch, R. E. An Adaptive Nonlinear Least-Squares Algorithm. *ACM Trans. Math. Software* **1981**, *7*, 348.

(45) Grosdidier, P.; Mason, A.; Aitolahti, A.; Heinonen, P.; Vanhamäki, V. FCC Unit Reactor−Regenerator Control. *Comput. Chem. Eng.* **1993**, *17* (2), 165.

(46) Han, I.-S.; Chung, C.-B. Dynamic modeling and simulation of a fluidized catalytic cracking process. Part II: Property estimation and simulation. *Chem. Eng. Sci.* **2001**, *56*, 1973.

(47) King, D. F. Estimation of Dense Bed Voidage in Fast and Slow Fluidized Beds of FCC Catalyst. In *Fluidization VI*, Proceedings of the International Conference on Fluidization, Alberta, Canada, 1989; Grace, R., Shemilt, L. M., Bergougnou, M. A., Eds.; Engineering Foundation: New York, 1989.

Received for review July 29, 2007
Revised manuscript received October 8, 2007
Accepted October 17, 2007

IE071035B